DEFENSE RESEARCH TECHNOLOGIES, Inc.

DRT TECHNICAL REPORT DR-025

DEVELOPMENT OF FLUIDIC GUIDANCE FOR KEW PROJECTILES

BY

TADEUSZ M. DRZEWIECKI
ALLEN B. HOLMES
EDWARD A. PACKARD
RAYMOND J. KIERNAN

DECEMBER 1988

SPONSORED BY

SDIO/INNOVATIVE SCIENCE AND TECHNOLOGY OFFICE

UNDER
CONTRACT DASG60-88-C-0081

MANAGED BY

US ARMY STRATEGIC DEFENSE COMMAND

354 Hungerford Drive, Rockville, Maryland 20852 (301) 762-3077/3078

REPORT DOCUMENTATION PAGE

READ INSTRUCTIONS BEFORE COMPLETING FORM

1. REPORT NUMBER	2. GOVT ACCESSION NO. / 3. RECIPIENT'S CATALOG NUMBER
4. TITLE (and Subtitle): Development of Fluidic Guidance for KEW Projectiles.	5. TYPE OF REPORT & PERIOD COVERED: Final Report
	6. PERFORMING ORG. REPORT NUMBER: DR-025
7. AUTHOR(s): Tadeusz M. Drzewiecki, Allen B. Holmes, Edward A. Packard, Raymond J. Kiernan	8. CONTRACT OR GRANT NUMBER(s): DASG 60-88-C-0081
9. PERFORMING ORGANIZATION NAME AND ADDRESS: Defense Research Technologies, Inc., 354 Hungerford Drive, Rockville, MD 20850	10. PROGRAM ELEMENT, PROJECT, TASK AREA & WORK UNIT NUMBERS: P63222C
11. CONTROLLING OFFICE NAME AND ADDRESS: Strategic Defense Initiative Organization, SD10/1st, Washington, D.C.	12. REPORT DATE: 30 Dec 88
	13. NUMBER OF PAGES: 75
14. MONITORING AGENCY NAME & ADDRESS (if different from Controlling Office): U.S. Army Strategic Defense Command, ATD, CSSD-H-V, P.O. Box 1500, Huntsville, AL 35807-3801	15. SECURITY CLASS. (of this report): Unclassified
	15a. DECLASSIFICATION/DOWNGRADING SCHEDULE: N/A

16. DISTRIBUTION STATEMENT (of this Report)

Distribution Unlimited

17. DISTRIBUTION STATEMENT (of the abstract entered in Block 20, if different from Report)

18. SUPPLEMENTARY NOTES

19. KEY WORDS (Continue on reverse side if necessary and identify by block number)

Fluidics, Laser Detectors, Diverters, Thrusters, Hot Gas Valves, Fluid Logic, Laminar Proportional Amplifier, Kinetic Energy Projectiles, SDI

20. ABSTRACT (Continue on reverse side if necessary and identify by block number)

Fluidic diverter valve and sensor technology could offer significant weight, countermeasure resistance and ruggedness advantages over conventional electronic or electro-mechanical guidance and control options provided that the valve thrust efficiency is sufficiently high to not be a limiting factor that offsets any weight benefits. This SBIR Phase I project brings together, in a unique and innovative combination, heretofore unexploited advances in

(continued)

20. continued

fluidic diverter valve efficiency and fluidic laser detectors. By being able to fluidically detect and demodulate coded laser guidance commands, highly thrust efficient fluidic thrusters can be individually addressed and a light-weight kinetic energy projectile, comprised essentially of only the fluidic circuit elements themselves, can be commanded to a hit-to-kill on a hostile ICBM booster.

A novel application of the photo-acoustic effect is used for laser detection. An acoustic wave, at the laser modulation frequency, is developed at the input of an acousto-fluidic amplifier when the laser energy impinges on a broadband absorber. Once the laser signals are converted into acoustic signals they are amplified and processed fluidically to produce high level pressure command signals that switch propellant gasses in a fluidic diverter to the desired thruster nozzle. High efficiency is achieved in the fluidic diverter valve by reducing the counter thrust produced by leakage flow. Four-way thruster efficiency is doubled over those concepts that must use two two-way thrusters because one half of the flow is not thrown away. No other approach to the guidance of KEW projectiles has ever considered a completely non-electronic solution which by its very nature would be completely insensitive to EMI or nuclear radiation, and by virtue of no-moving-parts will be as rugged as the basic materials would allow. Phase I showed that a 93%-efficient, dual-axis $10lb_f$ thruster combined with a demonstrated, 1 W/cm^2 sensitivity laser detector could be built for a weight penalty of less than 500 gm. The system would have a response time of less than 3 ms.

A fluidic package that makes up a lightweight, laser-guided "smart rock" could approach the lower limiting mass at the hypervelocities desired. A system of such low mass, high efficiency and fast response, could be the breakthrough needed to make EM railgun launch technology viable and would certainly increase the number of lethal projectiles available for a given payload in other space-based KEW applications.

DISTRIBUTION LIST

U.S. Army Strategic Defense Command
ATTN: CSSD-H-V (Mr. Mike Huhlein)
P.O. Box 1500
Huntsville, AL 35807-3801

U.S. Army Strategic Defense Command
Command Library
ATTN: CSSD-H-MPL
P.O. Box 1500
Huntsville, AL 35807-3801

Strategic Defense Initiative Organization
ATTN: IST (Mr. Carl Nelson)
The Pentagon
Wahington, DC 20301-7100

Institute for Defense Analysis
1801 North Beauregard Street
Alexandria, VA 22311

Defense Technical Information Center
Cameron Station
Alexandria, VA 22314

RSIC
Building 4484
Redstone Arsenal, AL 35898

TABLE OF CONTENTS

LIST OF FIGURES

LIST OF TABLES

ABSTRACT

In order for KEW projectiles to reliably destroy hostile ICBMs they must use some form of guidance. To be practical, KEWs must be lightweight, able to withstand high "g" forces, and insensitive to nuclear and electro-magnetic effects. Laser command guidance can guide a KEW to a target "basket" area whereupon a strapped-down seeker can guide for a hit-to-kill. Key elements of such a KEW system are a laser detector/processor and lightweight control thrusters.

Phase I demonstrated miniature photo-acousto-fluidic elements that detected, processed and demodulated FM laser signals riding on a 1.0 watt/cm^2 carrier. Using laminar digital fluidic logic, the ability to command "ON" or "OFF" any one of four thrusters was also demonstrated. In addition, high efficiency (>93%), 10-lb net force, single- and dual-axis fluidic diverter/thrusters, were designed and could result in a 300 - 500 gm fully guided KEW projectile.

Recommendations are made for Phase II efforts to build, test and demonstrate the diverters and to integrate a light weight detector. Brassboard cold and warm gas operation should also be demonstrated. The laser detection/processing circuitry needs to be designed to operate with propellant gasses. In order for the photo-acoustic detection process to operate efficiently and with high sensitivity, the detector element, as a minimum, must operate with cold gas (e.g. 500°R). Therefore it is recommended that a propellant gas bleed operating system with an integral heat exchanger be designed. High efficiency fluidic thrusters would be effective in any KEW, thus alternative activation means (tab, spark and fluid injection) should also be designed and demonstrated.

1. PURPOSE

This report has been prepared by Defense Research Technologies, Inc. (DRT) in fulfillment of its contractual obligations under a Strategic Defense Initiative Office (SDIO), Small Business Innovative Research (SBIR) contract, number DASG60-88-C-0081. The purpose of the report is to present the results of a feasibility analysis on the use of fluidic technology to provide both guidance as well as control of a kinetic energy weapon (KEW) projectile in order to reduce weight and cost, and to increase reliability and countermeasure resistance.

2. BACKGROUND

The first or "Boost" phase of the multi-layered Strategic Defense Initiative space-based protection concept, shown in figure 1, is to destroy Soviet ICBMs during their boost phase by lasers or kinetic energy weapon projectiles (KEWs) fired from satellites in orbit several hundred kilometers away.

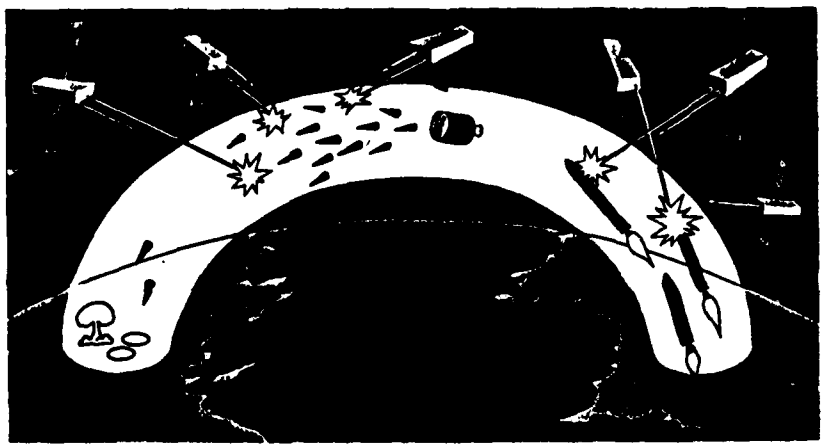

Figure 1. The multi-layered SDI concept.

The KEWs may be rocket-propelled or launched by electromagnetic railguns. In the case of EM gun launch accelerations in excess of 100,000 "g" may be expected in the process of getting the velocities up to 15 km/s and greater. In addition to having to survive incredibly high setback forces, the intelligence of any such "smart" projectiles would have to withstand incredibly high levels of induced magnetic effects. Currently, the EM gun is not in vogue, primarily because the energy required to launch the

relatively heavy, state-of-the-art KEWs is prohibitively large and the state of development of space-based homo-polar generators is not yet sufficiently well developed. The development, however, of lightweight KEWs, for example less than 1 kg in mass, may result in a re-evaluation of the practicality of the EM railgun as a launch mechanism and possibly their reinstatement in the principal SDI scenario.

KEWs, as are also expected to be used in the terminal phase defense. The High Endo-Atmospheric Interceptor or "smart rock", shown in figure 2 is illustrative of the Hughes concept.

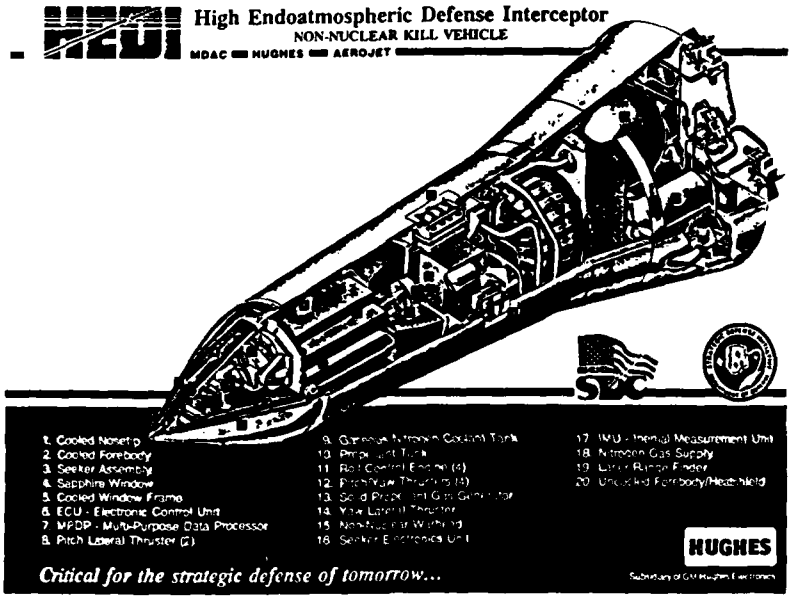

Figure 2. Hughes High Endo-Atmospheric Interceptor Concept

The KEW therefore forms an integral part of the lethality concepts for SDI.

In order for kinetic energy projectiles (KEWs) to hit and kill hostile ICBMs they must be guided. Guidance schemes available are command-guidance, terminal homing, or some combination of the two. Command guidance, by laser or RF beams, over distances of hundreds of kilometers to a point in space represented by a moving ICBM requires extremely high levels of pointing or tracking accuracy and very high resolution. At 100 km to be able to guide to within 1m would require a pointing accuracy of 0.01 milliradians. State-of-the-art platform stabilization and angular resolvers are not accurate enough. At the other extreme passive terminal homing (e.g. IR) from those great distances requires seekers and sensors with very high resolution and sensitivity. For example, a staring focal plane array with a 0.25 milliradian instantaneous field-of-view per pixel covers an area of 625 m^2 (25 m x 25 m) so

that a 1 m^2 hot spot has its effective intensity spread out over 625 m^2.

Currently conceived kinetic energy projectiles are highly complex, sophisticated homing devices that must operate as designed the first time. In order to do so, in addition to being highly accurate and lethal, they must be highly reliable, have a virtually indefinite shelf-life, and must be able to withstand hostile countermeasures and threats, as well as a variety of electromagnetic environmental effects, E^3, and nuclear radiation. One concept for a kinetic energy projectile is shown in figure 3.

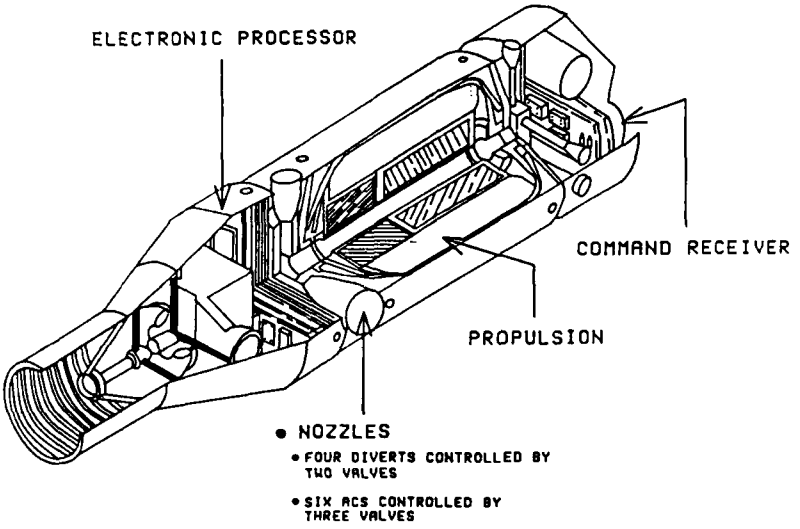

Figure 3. Conceptual SDI KE projectile.

The passive IR seeker guides the projectile to the target. Ten thruster nozzles, operated by three mechanical spoolvalves, provide the necessary control authority. Concepts such as these are stressed by weight and reliability constraints. The mechanical nature of the spool valves and the requirement to operate for as long as 100 seconds with extremely hot gasses (>5000°F) dictates relatively large, heavy, and bulky valves and consequently propellant. Propellant itself does not add to the kinetic energy that the projectile can deliver as it is consumed. Timelines are of the essence, so that merely flying at a slower speed to deliver a given level of kinetic energy is not an acceptable solution. Weights of current concepts, such as shown in figures 2 and 3, far exceed that required to kill an ICBM at the velocities required by the timelines.

The combination of the two guidance schemes, however, may be able to dramatically reduce the accuracy and resolution requirements, and consequently reduce weight and cost. One combination, that takes advantage of the best features of both command and homing guidance utilizes a laser command beam and strapped-down terminal homing. In this concept the projectile is guided by a coded laser beam to the target "basket", defined by the resolution and field-of-view capability of a small low-cost, two-dimensional focal plane array, whereupon the narrow field-of-view, strapped-down, staring IR array acquires the target at close range and guides the projectile in for the kill.

Two of the technical problems, therefore, driving KEW development are weight minimization and countermeasure tolerance. Weight growth of current concepts has stressed the delivery mechanism because the fly-off weight (mass) increases non-linearly with increasing propulsion demands (e.g. the heavier the projectile the more propulsive energy is required because not only the added mass must be accelerated but also the added propellant). Weight is adversely affected by any moving parts devices because they must be beefed up and ruggedized in order to meet the reliability and load requirements. The inherently complex electronics package, in order to be adequately tolerant of electronic countermeasure threats (jamming, directed energy weapons, etc.) and E^3, must be shielded or must use a redundant multiplicity of components. Shielding and redundancy add weight.

Fluidic technology addresses both of the above technical issues in a very direct manner. Fluidic devices have no moving parts and are inherently light in weight, rugged and immune to EM and nuclear effects. The spectrum of lightweight materials from which fluidic devices can be fabricated is considerably greater than for conventional mechanical valves, and the manufacturing methods used to produce systems of comparable accuracy and performance can be very low cost, compared to those used for precision, high temperature valves. Fluidic devices can accurately perform the sensing, signal processing and thrust actuation functions required in a KEW projectile.

Fluidic thrusters have been previously considered for SDI applications with mixed results. In general, they have not met with acceptance because of the relative thrust inefficiency of prior art diverter systems which has offset any weight advantages.

3. DEVELOPMENT OF FLUIDIC CONTROL PROOF-OF-PRINCIPLE DEMONSTRATOR

Defense Research Technologies, Inc. was awarded a Phase I SBIR contract to exploit recent technological advances in fluidics that could overcome previous limitations. Defense Research Technologies, Inc. developed proof-of-principle hardware and demonstrated the direct fluidic processing of laser energy using a unique adaptation of the photo-acoustic effect combined with advanced, second generation, solid-state, integrated circuit, laminar fluidic technology components. A unique, no-moving-parts, multi-axis, low flow consumption, fluidic thruster was also designed with a thrust efficiency of over 93 percent. The design was based on a single-axis valve which had demonstrated that level of efficiency but that had not been implemented in previous SDI concepts. The results of the diverter design effort are summarized in section 3.3. By eliminating all of the mechanically moving parts in a KEW and by reducing the number of electronic components that might be susceptible to electro-magnetic effects, significant reductions in overall projectile weight and size would be possible.

3.1 System Design Requirements and Parameters

The philosophy adopted in the development of this demonstration system was that all hardware should be directly translatable to flight hardware. Any differences in weight or size should be addressed solely by choice of materials and/or choice of manifolding. In other words, the demonstrator should be representative of the real thing in size, weight, response, and power consumption.

Four basic parameters were identified as being critical to an acceptable design -

* Laser Fluence
* Fluidic Output
* Response
* Power Consumption

The laser fluence that the projectile would have to sense was chosen to be 1 to 10 W/cm^2. This corresponds to levels that had been demonstrated as being readily detectable by fluidics and did not appear to be a power burden for a satellite-based laser that would be doing the command guidance. It also corresponds to the fluence available from commercially available 1 - 10mW HeNe lasers which were contemplated for use in the demonstration.

The goal for the fluidic output was chosen to be from 0.4 to 4 gm/s of air flow. This was based on the anticipated level of flow that would be required to switch a fluidic supersonic diverter valve that delivers 10 lbs of thrust. Assuming that the diverter operates most efficiently at a Mach number, M = 3 (see section 3.3 on the design of the fluidic diverter) and delivers sufficient

flow for a thrust of 10 lbs, then the diverter flow is roughly 40 gm/s. Assuming a switching efficiency or gain of 10 - 100, based on previous experience, then the laser detector circuit need deliver 0.4 - 4 gm/s.

The goal for the response time of the circuit was chosen to be 1 - 10 milliseconds. The choice of these values was arrived at by noting that a minimum of 100 control updates per second were thus possible and would be more than sufficient for high fidelity control. The values are consistent with the 3 - 5 ms response times being required for mechanical valves. The lower limit of 1 millisecond comes from the time it takes for the beam to move one half-width while tracking a booster 100 km away ascending at Mach 2.0.

The goal for power consumption of 5 - 10 watts was arrived at from an estimate of the consumption of an equivalent electro-mechanical system. This constitutes less than 0.01 percent of the available power from the 10 lb truster motor which would be used to power the fluidic circuitry.

The photo-acoustic detector and control system to address any one of four thruster control inputs was designed to be composed of five separate sub-systems -

* Laser detector
* Pre-amplifier
* Signal processor (D/A convertor)
* Four-state logic
* Impedance matching amplifiers (flow amplifiers)

For the demonstration a sixth element was designed to be the simulated thrusters themselves.

3.2 The Photo-Acoustic-Fluidic Detector and Pre-Amplifier

The photo-acoustic-fluidic detector is the device that directly converts electro-optical energy, in this case laser energy, into fluid power. In operation, incident electro-optical energy is converted into sound that is amplified and processed using advanced laminar acousto-fluidic signal processing techniques.

The photo-acoustic effect was discovered by Alexander Graham Bell[1,2] in 1880. He found that when chopped light is shined onto

---

[1] Bell, A.G., "On the Production and Reproduction of Sound by Light," Trans. American Assoc. for the Advancement of Science, 27 Aug 1880.

a broadband absorptive material such as carbon fibers, felt, or carbon black in an enclosed bell jar, audible tones can be heard at the chopping frequency. Bell called this phenomenon the "Photophone". Since the acoustic amplitude is proportional to the absorptivity of the target material, this phenomenon today forms the basis of the technology for the measurement of absorption properties of materials known as photo-acoustic spectroscopy[3].

When a pulse of radiation impinges on an absorptive material the radiant energy is converted into heat. Heating of the material itself occurs only in a very thin layer near the irradiated surface of the material. The heat is then rapidly conducted to the adjacent gas. The heating of the gas occurs in a thin thermal boundary layer in the immediate vicinity of the absorptive material. A small but rapid expansion occurs due to the local density decrease which develops an acoustic expansion pressure wave. The acoustic wave propagates away from the surface of the absorbing material and is available to be processed.

Bell Laboratory scientists developed an electrically passive photo-acoustic telephone receiver[4]. They demonstrated that a voice-modulated laser transmitted through several kilometers of optical fiber could be demodulated into speech in a photo-acoustic cavity. They were able to obtain a clearly audible, coherent and understandable sound output. Scientists at the US Army's Harry Diamond Laboratories (HDL), suggested that optical control signals could be demodulated and amplified by laminar acousto-fluidic amplifiers that would increase the acoustic output to levels where useful work could be performed. The HDL scientists built a pneumatic photo-acoustic fluidic interface demonstrator[5] and subsequently received a patent for a fluidic photo-acoustic detector[6].

---

2 Bell, A.G., "Upon the Production of Sound by Radiant Energy," Phil. Mag., Ser. 5, No. 11, 1881.

3 Pao, Y., ed., Optoacoustic Spectroscopy and Detection, Academic Press, NY, 1977.

4 Nelson, D.F., Wecht, K.W., and Kleinman, D.A., "Photophone Performance," J. Acoust. Soc. Am., Vol. 60, p. 251, 1976.

5 Gurney, J.O., "Photofluidic Interface," Trans. ASME, Journal of Dynamic Systems, Measurement and Control, Vol. 106, March 1984.

6 Drzewiecki, T.M., Gurney, J.O., and Toda, K., "Photo-fluidic Interface," US Patent No. 4,512,371, 23 Apr 1985.

Subsequent to the demonstration of the photo-fluidic conversion process in a pneumatic medium, Defense Research Technologies, Inc. demonstrated a similar capability in a hydraulic medium[7]. Optical signals of less than 10mW were successfully converted into high pressure hydraulic signals of greater than 100 psi.

Initial Phase I experiments were conducted to measure the critical performance parameters of the photo-acoustic cell itself, in order to establish the amplification requirements. The fact that the fluidic cavity is not sealed was of some concern and the initial assumptions were that the higher the impedance of the sensing device the higher would be the signal. Since amplifier size predominantly determines the impedance of the input, several experiments were conducted with amplifiers of differing sizes where three nozzle widths (size) were examined, b_s = 0.25, 0.1875, and 0.125 mm. A 1.0 mm diameter beam from a 10 mW HeNe laser was shined onto a 8mm focal length lens located some 8 mm from the graphite (carbon black) target located at the input of a C/2-format LPA. A microphone located at the rear of the LPA recorded the amplitude and phase of the acoustic pressure developed. The LPAs were operated with and without supply pressure. Without supply pressure the input channel resistance is governed by the outlet orifice area. For the sizes tested there was over an order of magnitude difference in impedance and yet the acoustic level varied only by as much as a factor of two. This implied that perhaps the source impedance of the photo-acoustic phenomenon is low compared with the impedance of the amplifiers. Using the data for the 510XX LPAs (b_s = 0.25 mm) at aspect ratios 0.5, 1.0, and 1.5 the source impedance was estimated. If one assumes that the equivalent circuit for the photo-acoustic phenomenon is represented by a series impedance connected to an invariant source then the pressure recovered (in fluidics pressure is analogous to voltage and volumetric flow is analogous to current) is a function of the load impedance, in this case the impedance of the input channel of the LPA as shown schematically in figure 4.

The ratio of pressure in the cavity to the source pressure is therefore given by:

$$P/P_S = 1/(R_S/R_L + 1) \quad \ldots\ldots\ldots\ldots\ldots\ldots\ldots \quad (1)$$

The ratio of two measurements of P, P_1 and P_2, for two different values of R_L, R_{L1} and R_{L2} yield the value for the source impedance R_S, such that:

$$R_S = R_{L1}\,[1 - P_1/P_2]/[P_1/P_2 - R_{L1}/R_{L2}] \quad \ldots\ldots \quad (2)$$

---

[7] Drzewiecki, T.M., "Research on the Direct Conversion of Electro-Optical Energy to Hydraulic Power," Defense Research Technologies, Inc. Technical Report DR-007, 16 Dec 1985.

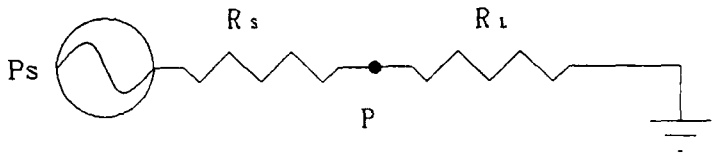

Figure 4. Schematic of photo-acoustic effect circuit.

For the measurements made, an average value of R_S = 5 T/LPM (convenient units of resistance are in torr/(liter per minute)) was found. This verified the initial observation that the source impedance must be low. Since the input impedances of C/2-format LPAs are generally of the order of 100 to 200 T/LPM it can be appreciated that the photo-acoustic cavity is operating almost as if it were a sealed volume. This was a very fortuitous discovery as it now permitted the use of the largest LPAs without degradation in performance. Since flow amplification is of interest starting with a high flow LPA reduces the staging requirements.

Figure 5 schematically shows the implementation of the laser detector stage and the two-stage 51009 pre-amplifier gainblock that was used to raise the signal levels for subsequent processing.

In order to eliminate any DC bias effects and to provide an output amplitude that was a function of frequency (a requirement for the operation of the D/A convertor) a third-order high-pass filter was included. This filter was composed of three pairs of RL (resistive/inductive) shunts each located at the outputs of the detector and the two amplifier stages.

The degree of amplification required was dictated by the signal level required to saturate a fluidic full-wave rectifier. Signal levels of 1.0 torr at the input to a 50710 fluidic rectifier operating at the same pressure as the 51009 LPAs (P_S = 16 torr) will saturate it. A pressure level of 1.0 torr corresponds to an acoustic level of 136.5 dB SPL (referenced to 0.0002 μbar). Since the input levels were of the order of 90 dB SPL a gain of 46 dB (200:1) was required. Three stages of self-staged LPAs yield a gain of 200 so that counting the detector element as one stage only two additional stages were required.

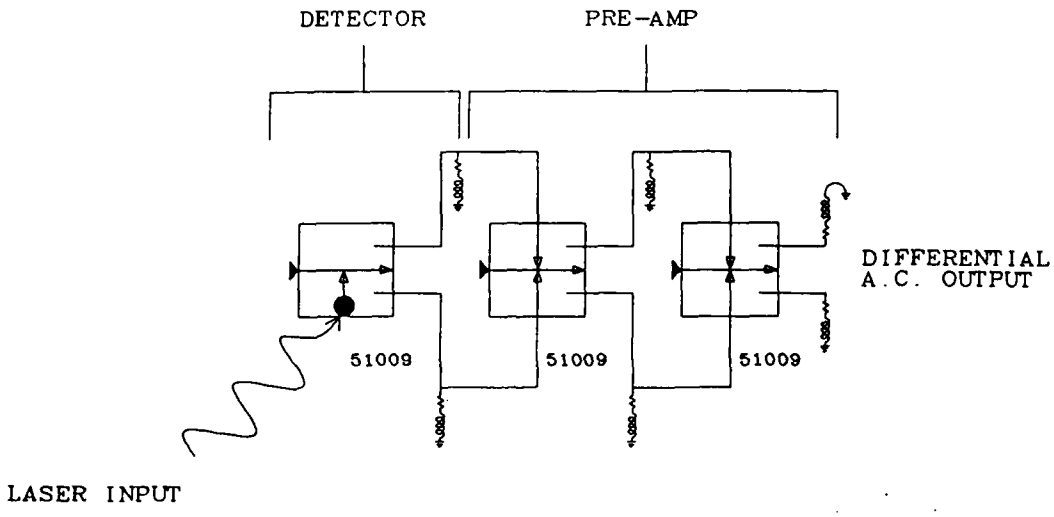

Figure 5. Detector/preamp/filter schematic.

Figure 6 shows the output waveforms of the detector/preamp/-filter at 1700 Hz and at three different supply pressures, 12.5, 15.0 and 18.0 torr.

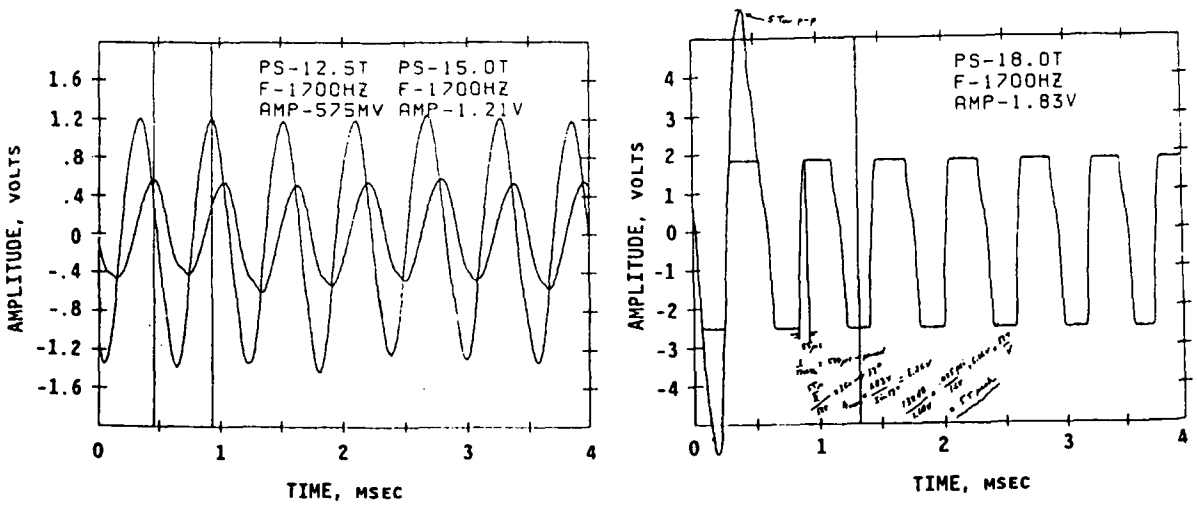

Figure 6. Laser detector/preamp output waveforms.

As supply pressure increases gain increases hence output amplitude also increases. At 18.0 torr the Knowles electret microphone is saturated at about 2 volts output. By measuring the time between positive and negative saturation points it was estimated that only 19% of the cycle was unsaturated (based on the assumption that the waveform was sinusoidal) and as a result the actual amplitude was estimated to be 6.26 volts corresponding to pressure amplitude of approximately 5.0 torr. This is more than sufficient to saturate the rectifier/signal processor stage.

Figure 7 shows the frequency response (variation of the ratio of the output amplitude to the input square wave driving the laser) of the sub-system with only a two-pole filter (the third-pole of the filter was actually implemented on the input of the rectifier element) for three supply pressures, 15, 16.5 and 18 torr.

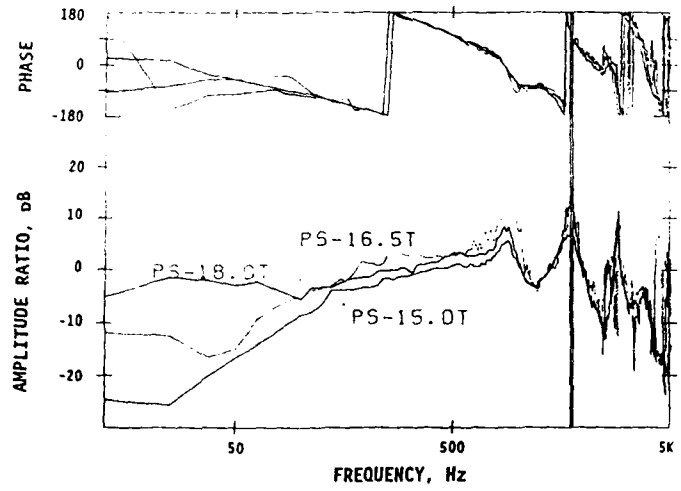

Figure 7. Detector/preamp frequency response.

The typically resonant nature of the high frequency end of the LPA is readily noted. Also of interest is the fact that there is responsivity out to 5000 Hz. The phase shift at 1000 Hz is seen to be about 360° which corresponds to a delay of 1 ms (millisecond). About 600 μs of that time is actual transport delay in the three stages.

3.3 Fluidic Signal Processor

The signal processing was a digital-to-analog (D/A) conversion of the AC output of the detector sub-system into an analog pressure level, proportional to frequency. By choosing four separate frequencies around a carrier, e.g. frequency modulating the laser, four output levels will be developed which will then be identified by a logic circuit and will produce separate signals to drive the thruster. The process by which an analog pressure is produced from an AC or acoustic pressure is rectification. If the input amplitude at different frequencies is different then the analog output will be a function of frequency. The high-pass filter provides the variation of input amplitude versus frequency.

A silhouette of a full-wave rectifier is shown in figure 8 below.

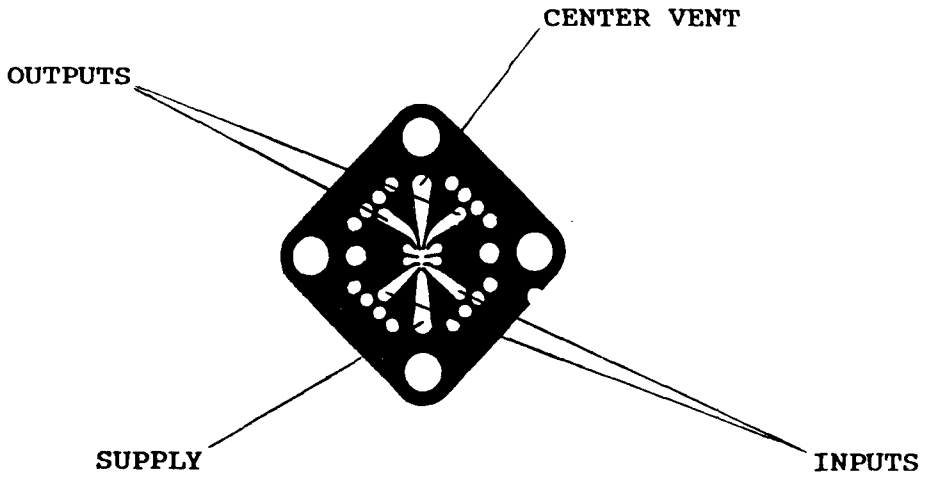

Figure 8. Silhouette of a fluidic full-wave rectifier.

When a differential sinusoidal signal is impressed on the controls the output of each leg produces a positive pulse only when the flow is impinging on it. Each output is out of phase with the other. These two positive pulses are summed in a passive resistive summing junction to produce the absolute value of the input signal. When low-pass filtered the result is a DC level. A schematic of the circuit used is shown in figure 9.

The low-pass filter is implemented by a small volume that acts as a capacitance-to-ground. Using 500 T/LPM resistors a volume of 300 mm^3 is required.

Figure 10 shows the analog DC pressure developed by the rectifier circuit when loaded into the logic circuit (to be described in the following section).

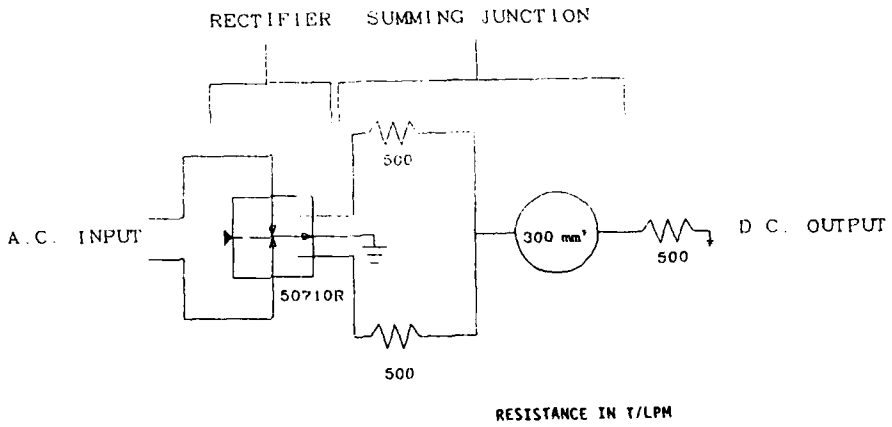

Figure 9. Rectifier schematic.

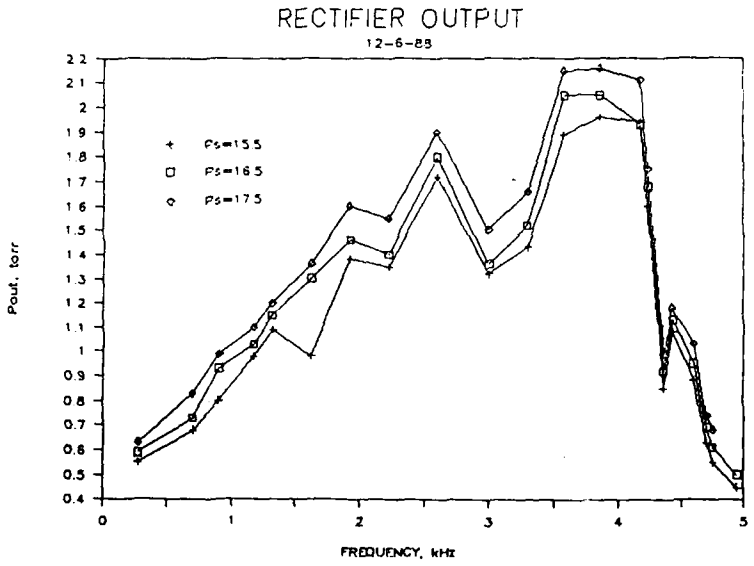

Figure 10. Analog output versus frequency.

A variation of from 0.5 to 2.1 torr is achieved for input frequencies from 500 to 5000 Hz. Using a 4kHz carrier, where the peak output occurs, the option of modulating down 3kHz or up 1kHz is allowable.

The power consumption is computed as the product of the pressure and flow at the operating point. Each stage of LPA operating at about 16 torr (2160 Pa) with a flow consumption of 0.15 LPM (2.5×10^{-6} m^3/s) consumes 5 mW of power. Therefore the four active elements comprising the detector, preamp, and the rectifier consume a total of 20 mW.

3.4 Four-State Logic Circuit

The design of the logic circuit was geared around a four-state logic tree that produced output commands from four outputs in response to four analog signal level inputs. The logic that was desired is described in the following truth table:

Table 1. Four-State Logic Truth table

Input Level	Output O1	O2	O3	O4
1	ON	OFF	OFF	OFF
2	OFF	ON	OFF	OFF
3	OFF	OFF	ON	OFF
4	OFF	OFF	OFF	ON

Based on the rectifier output results the switching levels were chosen as follows:

Table 2. Logic Level Definitions

Input Level	Analog Pressure (torr)	Frequency (Hz)
1	0.6	4700
2	1.0	4600
3	1.3	4250
4	1.8	4100

The principal laminar logic element is composed of a two-stage LPA where the first stage is a proportional amplifier with positive-feedback to drive it into digital saturation. The second stage is merely a buffer that isolates the feedback resistances from any loading effects. Figure 11 shows the schematic implementation of such a digital device.

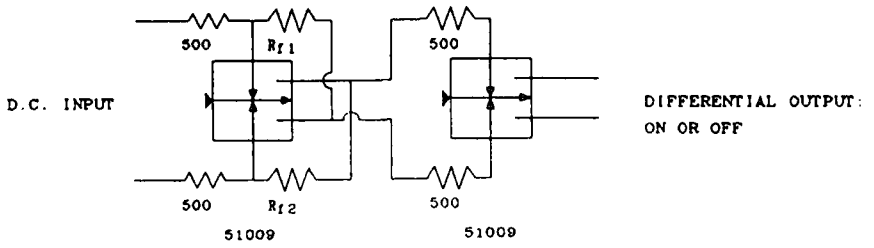

Figure 11. Schematic of a laminar logic element.

In keeping with a desire (for convenience only) to use only one supply pressure, the logic elements were chosen to be 51009 LPAs as in the detector/preamp. The feedback, load and input resistances can be computed for the case where the gain of the device becomes infinite, e.g. the case where there is no hysteresis. Drzewiecki[8] has shown that these resistances can be computed by examining the functional form of the gain of the device. Equation 3 gives the desired relationship.

$$R_f = \frac{GR_i - R_i - R_o - R_iR_o(1/R_d + 1/R_L)}{1 + R_i/R_d + R_o/R_L + R_iR_o/R_dR_L} \quad \ldots\ldots \quad (3)$$

where for the 51009 LPAs used -

G -	LPA blocked pressure gain,	G = 10
R_d -	deflection resistance,	R_d = 100 T/LPM
R_o -	output resistance,	R_o = 60 T/LPM
R_i -	input resistance,	R_i = TBD
R_L -	load resistance,	R_L = TBD
R_f -	feedback resistance,	R_f = TBD

Given that the circuit resistances are free parameters they were chosen based on the standard available values. The 5412 resistor, a silhouette of which is shown in figure 12 is a capillary resistor with a length of 15 mm, a width of 0.254 mm and a lamination thickness of 50 μm (0.002 in).

---

[8] Drzewiecki, T.M., "Dual Mode Reaction-Jet, Thrust-Vector Controls for Small Missiles," J. of Guidance and Control, Sep 1984.

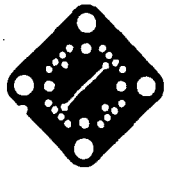

- RESISTOR LAMINATIONS - 50 MICRONS THICK
  250 MICRON CHANNEL

1-LAMINATION	=	10,000 T/LPM
2-LAMINATION	=	1,500 T/LPM
3-LAMINATION	=	500 T/LPM
4-LAMINATION	=	250 T/LPM
10-LAMINATION	=	50 T/LPM

Figure 12. Fluidic resistor lamination.

Different values of resistance can be obtained by either stacking laminations to increase the depth of the channel or by paralleling various combinations of stacked resistors. Table 3 lists the resistance values achievable by stacking.

Table 3. Standard Resistances

No. of Laminations	Resistance (T/LPM)
1	10,000
2	1,500
3	500
4	250
5	100
10	50

When the input and load resistances are chosen to each be 500 T/LPM and the feedback is 750 T/LPM, a flip-flop is formed with a hysteresis loop width of approximately 0.25 torr (e.g. switching pressures are ± 0.125 torr). This flip-flop can be changed into a NOR-gate by changing the feedback resistances on either side relative to themselves. The hysteresis width will stay constant when the average of the two feedback resistances remains constant. The switching pressure will increase the larger the difference in feedback resistances.

The truth table (Table 1) was implemented by using the logic circuit shown in figure 13.

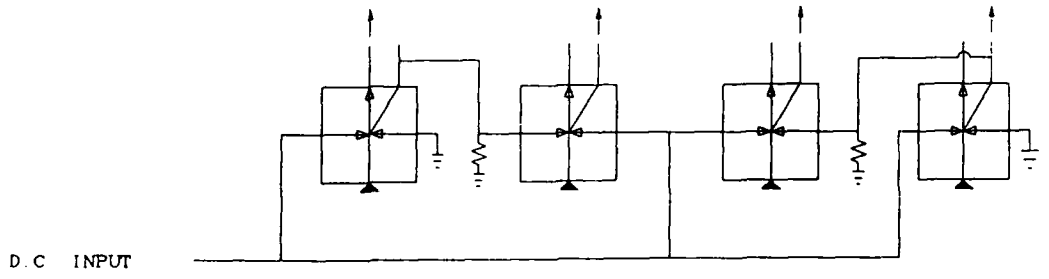

Figure 13. Logic circuit.

The first NOR-gate is set to switch off at about 0.8 torr. When the initially OFF leg switches ON that pressure is used to switch the second NOR-gate ON. In this manner it is guaranteed that when either one is ON the other is OFF. Gate 2 is switched OFF when the control pressure applied to the opposite control exceeds 1.3 torr. The third NOR-gate switches ON when the control pressure exceeds 1.3 torr and is turned OFF by bleeding off from the ON output of the fourth gate when it switches ON. Figure 14 schematically shows the implementation of the logic circuit of figure 13 using the two-stage logic elements described in figure 11.

Figure 15 shows the output states of the circuit of figure 14.

Note that the OFF values of the outputs are not at zero pressure. As a result biases are developed on the inputs of the logic elements that are turned ON or OFF by another logic element. This was accommodated by adjusting the individual switching characteristics of each NOR-gate. For example, the third gate must be turned ON by a control level of 1.3 torr but must overcome a bias level of about 1.0 torr that is present from the OFF leg of gate 4. The switching level of gate 3 therefore had to be set at 0.3 torr. The switching levels are accurate to within ±0.1 torr for a ±10% variation in the supply pressure.

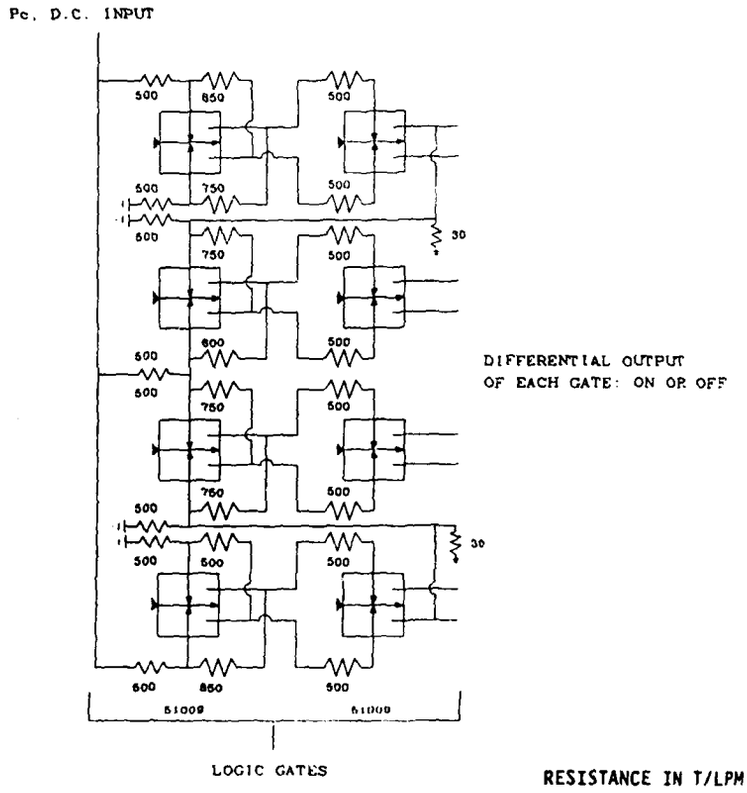

Figure 14. Schematic of the implemented logic circuit.

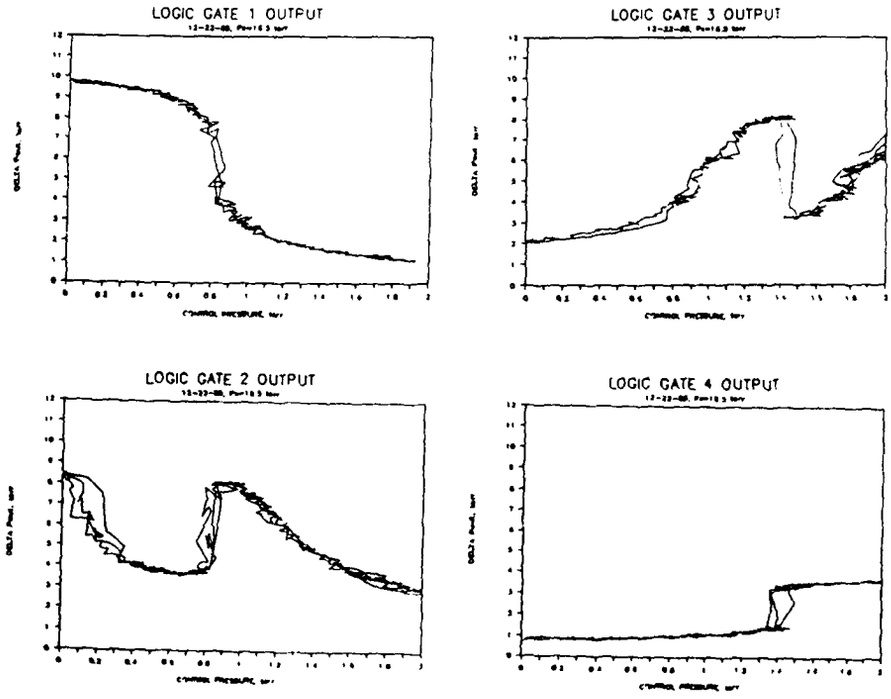

Figure 15. Logic circuit performance.

The switching time is the time required to drive the fluid streams in the two LPAs into saturation. Drzewiecki[9] has shown that the large-signal propagation delay, τ, associated with the saturation of a single LPA is equal to four transport delays across the amplifier.

$$\tau = 4\, x_{sp}/[c_d(2P_s/\rho)^{\frac{1}{2}}] \quad \ldots\ldots\ldots\ldots\ldots\ldots \quad (4)$$

where -

x_{sp} - nozzle-to-splitter distance, 0.002 m
c_d - discharge coefficient, dimensionless, ~ 0.7
P_s - supply pressure, ~ 2160 Pa
ρ - fluid density, 1.2059 kg/m^3

The switch time of one element is 190 μs and of two in combination the total switching time is approximately 380 μs. Only one logic element switches at any one commanded pressure level hence the switching time for any command is 380 μs.

The logic circuit is composed of eight LPAs so that the power consumption is 40 mW.

3.5 Impedance Matching (Flow) Amplifiers

The ON pressure levels developed by the logic circuit of between 8 and 10 torr are developed into an infinite impedance load. The maximum flow available from an ON output is about one hundred times too small to drive a diverter (e.g. 0.4 to 4 gm/s). These mass flow rates correspond to 20 to 200 LPM at atmospheric pressure. The demonstration thrusters (see section 3.2.6) will be capable of delivering the required flow to the vortex thrusters so that a matching amplifier was designed to match the logic outputs to the turbulent wall attachment amplifiers used for the demonstration. This was accomplished by a two-stage gainblock composed of three parallel 51010 LPAs for the first stage and ten for the second stage. This effectively provided a factor of ten reduction of the output impedance and increased the output flow at saturation by a factor of ten. Figure 16 shows the circuit schematic and figure 17 shows the DC pressure gain transfer characteristic for five different supply pressures showing that the pressure gain is supply independent.

Since there are thirteen LPAs in each of four matching amplifiers the power consumption of 52 LPAs is 260 mW.

The switch time of 380 μs is the same as for the two-stage logic gates.

---

[9] Drzewiecki, T.M. "A Fluidic Voice Communication System and Datalink," Dr. Eng'g. Thesis, US Naval Postgraduate School, Mar 1980.

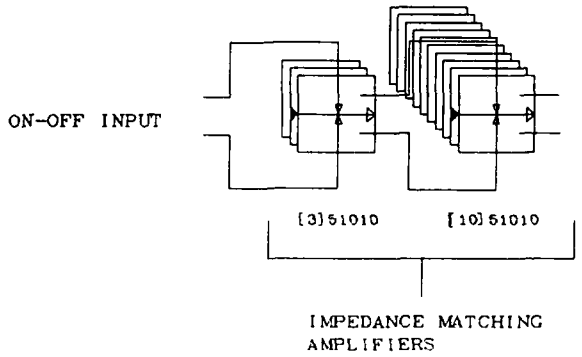

Figure 16. Schematic of matching amplifier.

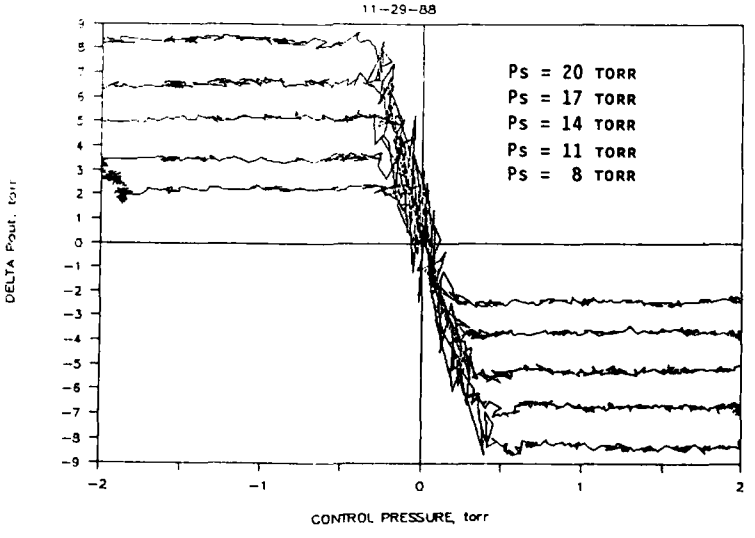

Figure 17. DC pressure gain transfer characteristic of the matching amplifier.

3.6 Demonstration Diverters (Diverter Interface Amplifiers)

The power output of the fluidic circuit can be generated by using first generation turbulent Coanda effect flip-flops. These devices have supply nozzles that are 0.76 mm wide and 1.5 mm high (aspect ratio, σ = 2). At a supply pressure of 10 psig a saturated output will deliver 0.4 gm/s. For the purposes of the demonstration the flip-flops were operated at the system supply pressure of 16 - 18 torr which was sufficient to flutter ribbons to provide a visual output of the thruster operation. Figure 18 shows the outputs of the turbulent amplifiers in response to the DC analog control pressure from the rectifier circuit.

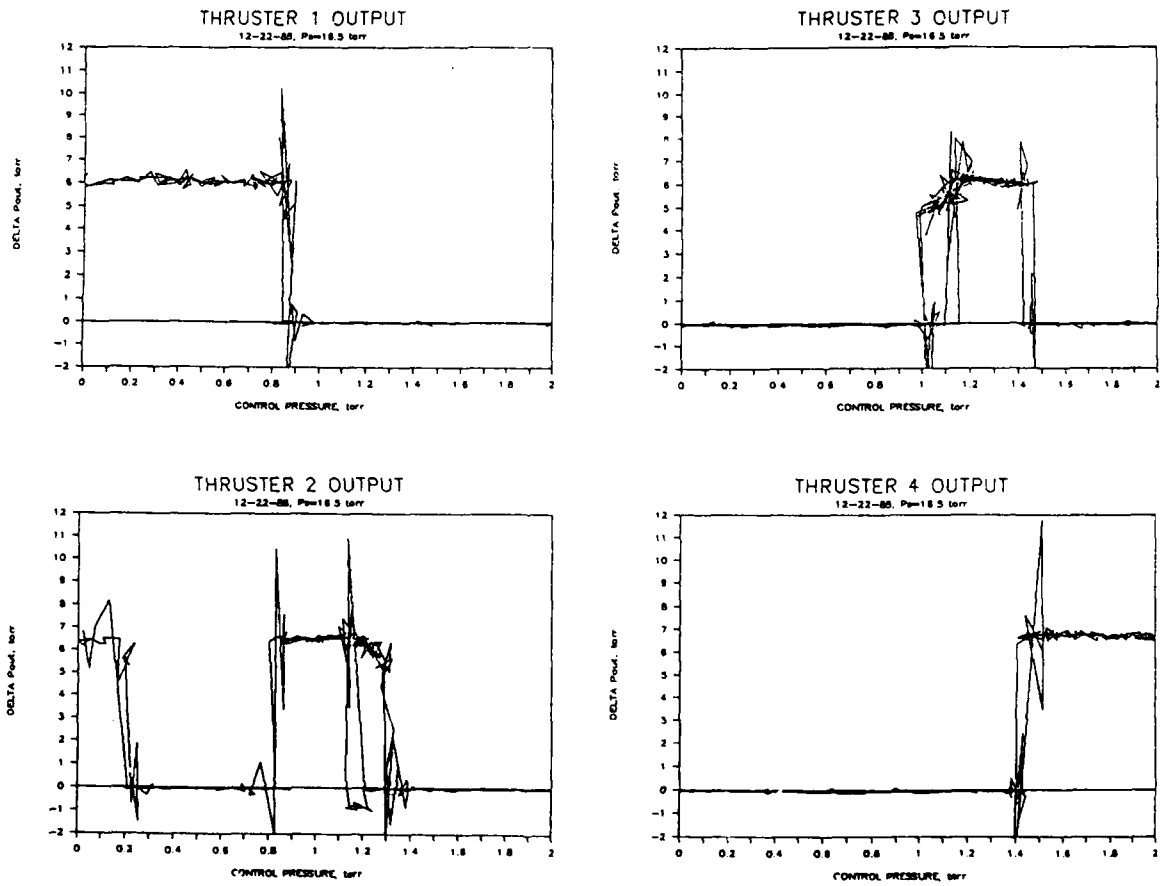

Figure 18. Thruster output characteristics.

Turbulent Coanda devices are relatively much slower, in terms of the number of transport times it takes to switch, than a laminar device primarily because of the large capacitive load of the Coanda attachment bubble. These devices require over ten transport times to switch. At the operating pressure of 10 psig required to develop the amount of flow to switch the supersonic diverter, the switch time is about 320 μs (this is faster than the logic elements because the velocity is higher and the transport time is faster).

3.7 The Integrated Demonstration Circuit

Figure 19 shows the circuit schematic for the complete demonstrator system.

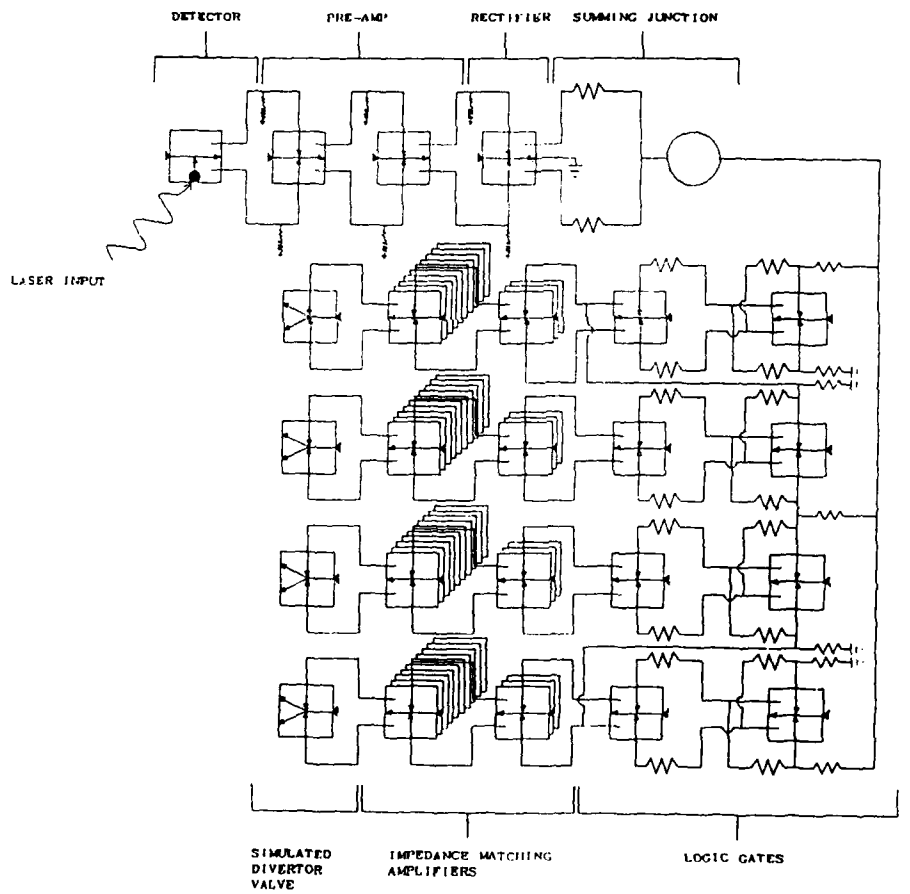

Figure 19. Demonstrator system circuit schematic.

Figure 20 shows silhouettes of the active elements actually used to build the system.

- LASER DETECTOR/1ST STAGE AMPLIFIER
  NOZZLE WIDTH - 0.254 MM (0.010 IN)
  ASPECT RATIO - 0.9 (51003 (3) - CONFIGURATION)

- METAL-ETCHED AMPLIFIER LAMINATIONS
  51003 CONFIGURATIONS - SIGNAL PROCESSING
  51005 CONFIGURATIONS - POWER ELEMENTS

- METAL-ETCHED FULL-WAVE RECTIFIER LAMINATION
  50703 CONFIGURATION

Figure 20. Active fluidic elements.

The integrated circuit was assembled as shown in figure 21.

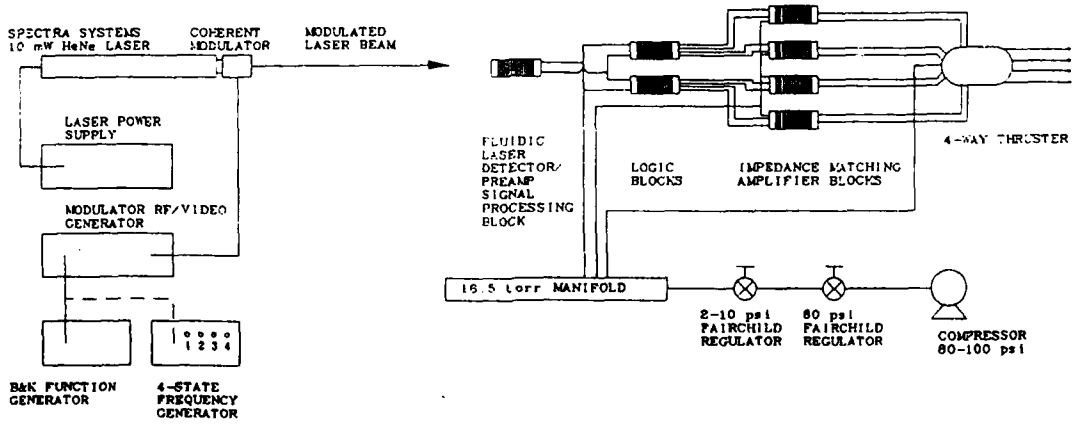

Figure 21. Brassboard demonstrator schematic.

The fluidic circuit is composed of eight modules. The first module contains the detector, pre-amp, and signal processing circuitry. The next two modules comprise the logic circuitry. Logic gates 1 and 2 are in one module and logic gates 3 and 4 are in the other. Each of the four matching amplifiers is contained in a separate module. The final module is composed of the four Coanda flip-flops. The entire circuit is supplied from a single source pressure of between 16 and 18 torr which is obtained from a compressed air source that is double regulated.

The electronic side of the brassboard is composed of the laser and modulation circuitry. The laser is an off-the-shelf Spectra Systems 10 mW HeNe CW laser. A square wave carrier is impressed by a Coherent Systems acousto-optical modulator driven by either a B&K Function Generator or by a special four-state frequency generator custom built for the demonstration.

Figure 22 shows two photographs of the brassboard system in operation. The ribbons at the ends of the nozzles are caused to flutter out when the thruster is turned on.

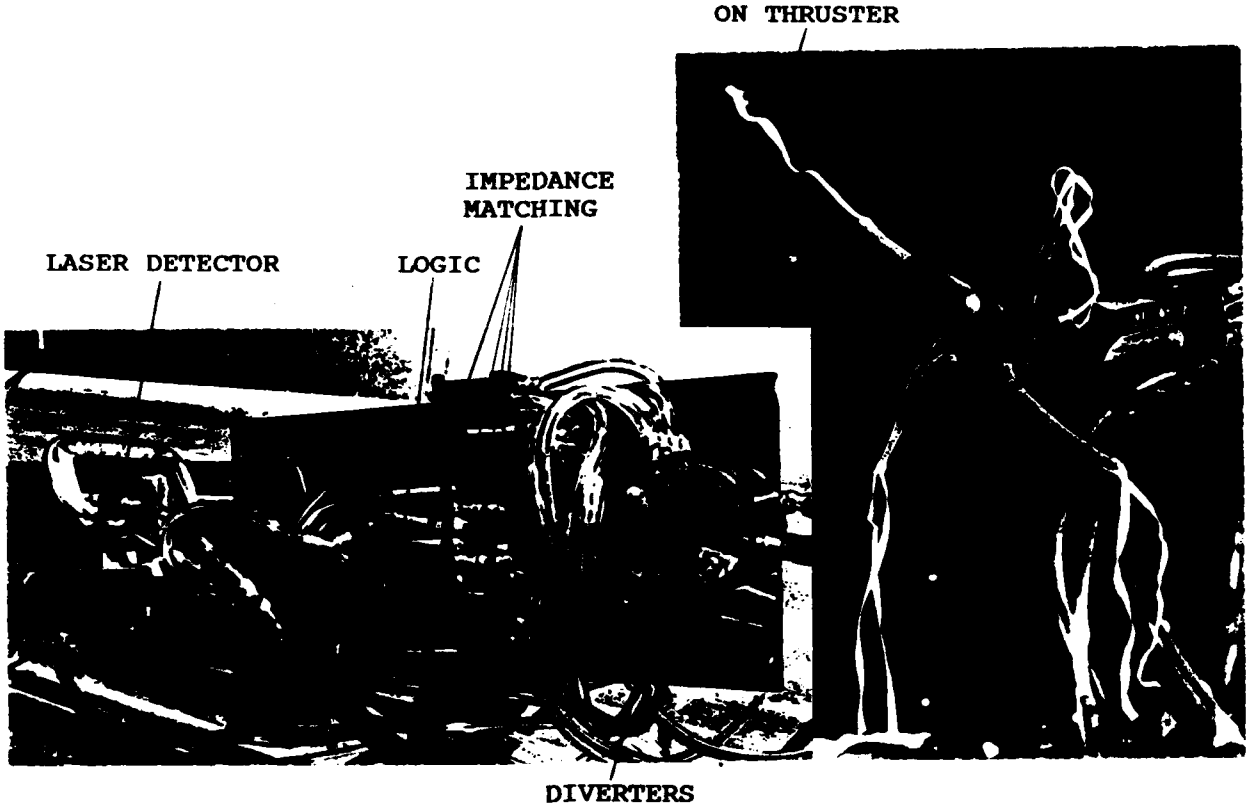

Figure 22. Photographic sequence of operating brassboard.

Table 4 is a summary of the brassboard performance.

Table 4. Brassboard Demonstrator Performance

Parameter	Measured	Design Goal	Met Goal
Laser input (W/cm^2)	1.0	1 - 10	YES
Threshold (W/cm^2)	0.1	-	-
Carrier frequency (kHz)	4.0	0.1 - 20	YES
Modulated frequency (kHz)	1.0	0.01 - 2	YES
Sensitivity (torr/Hz)	0.0015	-	-
Response (ms)	2.1	1 - 10	YES
Signal Processing Power consumption (W)	0.32	5 - 10	YES
Actuation Power consumption (W)	0.44	-	-

As can be seen from the above table the design goals were all met or exceeded. The power consumption of well less than 1 watt was a very pleasing result as was the very fast response.

3.8 Projected Performance/Characteristics of Flight Hardware

The dynamic and power consumption performance characteristics identified by the brassboard system are expected to be more than adequate for flight hardware. The only parameters not demonstrated explicitly by the brassboard system are size and weight. The volume of the brassboard elements, less the thrusters, was 5.2 in^3 (85 cm^3) and the thrusters/actuators was 8 in^3 (130 cm^3) for a total volume of just over 13 in^3 (215 cm^3). Without any further optimization the entire system (e.g. a complete laser-guided KEW projectile) could conceivably be put together into a cylindrical package approximately 1.5 in in diameter and 1 ft long. If the package were to be constructed from the same stainless steel as the brassboard the mass would be about 1.3 kg. It is anticipated that flight hardware materials will be carbon/carbon composite having a density roughly one-quarter that of steel. Graphite fluidic laminations have been made successfully in the past and as such no problems would be anticipated. A graphite circuit would have a mass of about 0.33 kg. Graphite, as the baseline material, has the added advantage that no special target material would have to be introduced for sensing the laser signals.

Optimization of the volume could occur most efficiently in the turbulent Coanda devices where the volume could easily be reduced by a factor of ten from that used in the brassboard. A 10-percent reduction of the volume of the laminar circuitry probably is possible without major changes to the circuit topology or construction format. A 6.0-in^3 package with a mass of about 0.15 kg may be feasible.

3.9 Technical Challenges Identified

The photo-acoustic effect operates on the principle of heating a gas to generate an acoustic pressure wave. For a given level of energy deposited the temperature rise is approximately the same regardless of the ambient temperature as shown simplistically in eq. 5. The product of the mass, specific heat and the change in temperature defines the change in energy input that is required to achieve that temperature change.

$$dE = m\, c_p\, dT \quad \ldots\ldots\ldots\ldots\ldots\ldots\ldots\ldots \quad (5)$$

However the change in gas density due to a change in temperature can be approximated from the perfect gas law and shows that as the ambient temperature, T, increases the change in density, $d\rho$, decreases.

$$d\rho = - p\, dT/[RT^2] \quad \ldots\ldots\ldots\ldots\ldots\ldots\ldots \quad (6)$$

where -

- dE - change in energy, joules
- m - mass, kg
- c_p - specific heat, J/kg/°C
- T - temperature, °C
- dT - change in temperature, °C
- ρ - density, kg/m^3
- p - pressure, Pa
- R - gas constant, $m^2/s^2/°K$

Since acoustic amplitude is directly proportional to the change in density it follows that the higher the temperature the smaller the sensitivity of the photo-acoustic detection process.

The gas supply in a KEW projectile may come from the burning propellant, in which case it will be very hot, or from an onboard gas bottle, which will increase the mass of the projectile. Clearly it would be advantageous to use the products of combustion as the working medium. The thruster/diverters will, of course, be operating with the hot gasses. The thruster actuators could also operate with the hot propellant gasses without any loss in the generality of the analysis and design performed. The laminar circuitry and, specifically, the detector, may be better operated at low temperatures. Operating at low temperatures also has the advantage of eliminating any materials toughness considerations. The development of a bleed and cooling manifold should be examined, perhaps using Joule-Thompson or radiative cooling.

The burning propellant can be designed to develop a fairly constant pressure, generally varying less than 20% over the burn period by appropriate grain design. The signal processing fluidics really need regulation to about 5% so that some consideration of a simple fluidic pressure regulator needs to be made.

4. THE DESIGN OF THE FLUIDIC DIVERTER VALVES

Diverter valves are used to control the high temperature propellant gasses delivered to KEW projectile attitude control and divert propulsion thruster nozzles. These valves must be fast acting, extremely light weight and must require very little on-board power to operate. This Phase I effort analytically demonstrated the feasibility of a fluidic diverter valve capable of diverting propellant from a single source to up to four thruster nozzles.

Diverter valves are used to control both ground-launched and space-launched kinetic energy projectiles. Conventional diverter are electro-mechanical devices that are heavy, require a considerable amount power to actuate them, and have relatively slow response. Fluidic diverters are fluid dynamically controlled devices that contain no-moving-parts, require very little actuation power, and have a speed of response limited only by the transport time of fluid through the valve body. In a typical, conventional electro-mechanical diverter valve system, one valve is required per control axis to divert flow between two opposing thruster nozzles. In a complete mechanical diverter system five diverter valves are used to supply flow to ten nozzles which produce control forces in the pitch, yaw, roll and diverts directions. By comparison only three fluidic diverter valves would be required to perform the same functions.

Fluidic diverter valves have been analyzed, designed, built, tested, and evaluated over the last 27 years by many Army and industrial organizations including: the US Army Harry Diamond Laboratories (HDL), United Aircraft (UAC), Aeronutronic Ford, the US Army Missile Command (MICOM), US Army Armament Research, Development and Engineering Center at Picatinny Arsenal, Martin Marietta, Chandler-Evans (Colt), Garrett Industries, and Plessey Aerospace. Table 5 shows the contributions of these agencies in a historical trace of the developmental process of the state-of-the-art in fluidic diverter valves.

Important developments illustrated in Table 5 include the type of valve (2-way, 3-way, 4-way, or secondary injection thrust vector control - SITVC), the type of testing (cold gas, warm or hot gas with maximum temperatures, static firing, or flight test), and efficiency based on maximum recovered thrust.

Two-way and four-way fluidic diverter valves were first introduced by the Diamond Ordnance Fuze Laboratories (DOFL), now called the Harry Diamond Laboratories (HDL) in 1960. Basically these diverters employed supersonic amplifiers to divert a high velocity gas stream directly into thruster nozzles. Thrust efficiency was measured at about 65% in cold gas testing. In 1964, HDL flight tested a four-way supersonic fluidic amplifier diverter valve, shown in figure 23, in a modified Little John

missile[10]. This valve provided dual-axis control (pitch and yaw) using a single supersonic amplifier to divert propellant gas between two opposing pairs of outlet nozzles. Related work was also performed on a secondary injection thrust vector control (SITVC) valve.

Table 5. Fluidic Hot Gas Valve History

ORGANIZATION	PROGRAM	DATES	VALVE TYPE	ALTIT. INSENS	TESTING	EFFIC.(%)
HDL	R&D	1960-1965	2/4-way & SITVC	NO NO	Cold Gas Flight	65 65
UAC	Polaris	1962	SITVC	YES	Hot Gas (5800°F) Static Firing	NA
Aeronutronic Ford	IR&D	1963-1964	2-way (Vortex)	YES	Warm Gas (2100°F) Static Firing	94
MICOM	R&D	1965	2-way & SITVC	NO	Warm Gas Flight	65
ARDEC/HDL	R&D	1965	2/4-way & SITVC	NO	Hot Gas (5300°F) Flight	65
Martin Marietta	SPRINT ABM	1975	SITVC (Vortex)	YES	Hot Gas (4200°F) Static Firing	NA
Chandler Evans (Colt)	TANK BREAKER	1983	3-Way	NO	Hot Gas Flight	65
Garrett	SDI KE Others	1988	2-way (Vortex) 4-way	YES	Warm Gas (2100°F) Flight	65-75
Plessey	SDI KE	1988	---	YES	---	--

While great strides were made, the principal problems with these early valves was their limited usefulness because of their sensitivity to variations in external ambient pressure with altitude. The need to isolate the supersonic amplifier from low external pressures, in order to provide altitude insensitivity, spurred Aeronutronic Ford in 1963 to design a new two-way fluidic diverter valve. Vortex triodes were added at the outputs and connected by a cross-over channel for bleed flow from the active thruster leg to provide greater off-leg shut-down and very low leakage flow from the inactive (non-flowing) thruster. In warm gas tests this design was demonstrated to have a thrust efficiency of 94%. A schematic of the device is shown in figure 24.

---

[10] Holmes, A. B., "Development Report on a Fluid Amplifier Attitude Control Valve," Proceedings of the 2nd Fluid Amplification Symposium, Oct 1965.

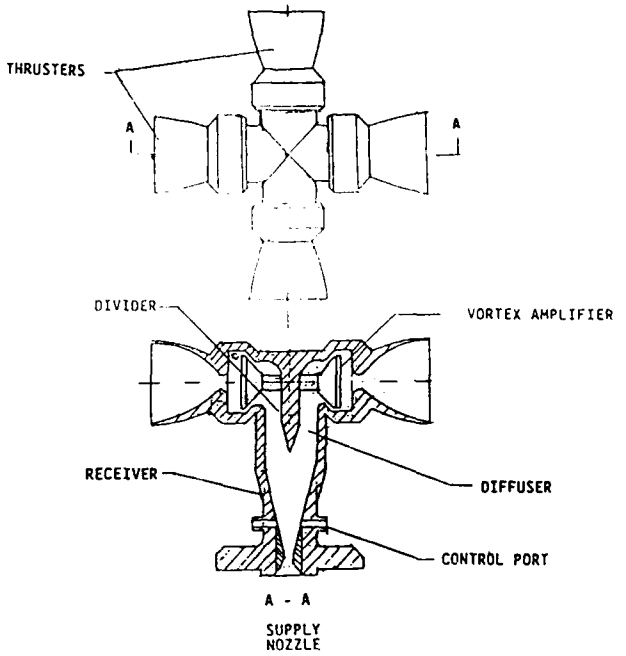

Figure 23. HDL four-way fluidic diverter valve.

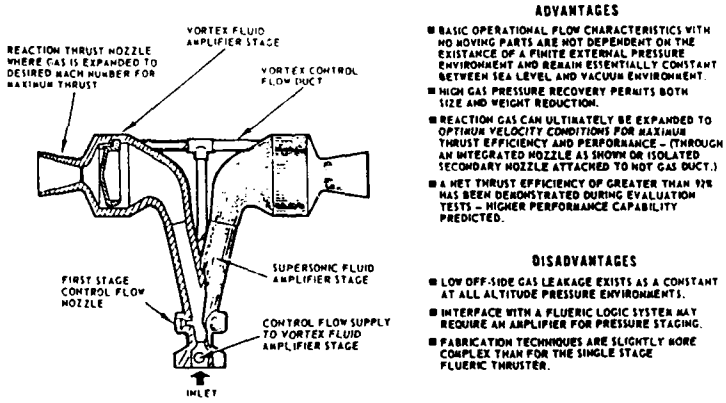

Figure 24. Schematic of the Ford single-axis diverter.

A valve with operating characteristics similar that described above designed built and hot gas tested by Ford[11]. The valve was actuated using secondary injection, spark discharge and tab insertion. The valve was reportedly insensitive to changes in ambient back pressure and operated at an efficiency level of over 92-percent. Higher efficiencies were predicted for more optimized valve designs.

In the late 1960's, another altitude insensitive fluidic amplifier with vortex valves was introduced by the Garrett Corporation. These devices formed the basis of the fluidic valve concepts examined for SDI applications. The Garrett diverter valve used electro-mechanically actuated amplifiers to control the flow to the vortex valves to switch the propellant flow to the thruster nozzles on and off. The vortex valves isolated the fluidic amplifiers from the atmospheric environment. These diverters operate at a constant flow in a push-pull mode but because the control flow is used to shut off the main propellant flow this flow is significantly higher than the control flow in the Ford concept which only needs to shut off a small leakage flow, resulting in efficiencies of about 80% or less.

Garrett has been involved with developing two-way and four-way fluidic diverter valves for use in a wide variety of control applications including those on the LEAP and SAGITTAR KEW vehicles.

The combination of the Ford isolation and efficiency improving concept with the four-way diverter (figure 23) forms the basis of a unique approach to the development of a dual-axis system that overcomes all of the efficiency problems of previous fluidic diverters. It is such a dual-axis valve that has been the subject of this Phase I effort.

The development of highly efficient fluidic hot gas diverter valves, by itself, could represent the advancement in hot gas valve technology that is needed to meet anticipated KEW vehicle propulsion system, weight, response, power and reliability requirements. For example significant reductions in weight would be achieved by using one instead of two valves to pressurize four nozzles arranged to produce control moments about the pitch and yaw axis. Additional weight saving may be made possible by locating the fluidic diverters inside the gas generator. Such an arrangement would place the valve structure in compression allowing the use of thinner walled materials and higher operating propellant gas pressures. Locating the valves inside the gas generator would also reduce thermal gradients in the valve structure and reduce radiant heating effects inside the KEW vehicle where other critical components are required. Other weight saving would result from

---

[11] Fix, John, "Flueric Altitude Insensitive Thruster," ASME paper presented at the 1969 ASME Winter Annual Meeting.

the ability to actuate the valves with low power levels therefore reducing the power supply requirements for operating the valves.

When the opto-fluidic laser control technique is used in conjunction with fluidic diverters, a unique, extremely rugged, reliable, no-moving-parts, non-electronic attitude control system is formed which will respond to coded laser beam commands transmitted to a KEW vehicle from a satellite station. These commands are demodulated by opto-fluidic interface circuits and converted into pressure/flow signals that actuate the diverter. The diverter responds and produces control forces which guides the projectile to the target. The components used to form the system and diverter valve structures could also be an integral part of the KEW vehicle structure. In addition, these fluidic circuit structures can be easily hardened against the anticipated launch electro-magnetic and acceleration environment and nuclear weapons radiation effects encountered during an engagement.

This Phase I effort focussed on the design of light weight fast acting, low power two way and four way hot gas fluidic diverter valves. A conceptual drawing illustrating both two way and four way fluidic diverter valve structures is presented in figure 25.

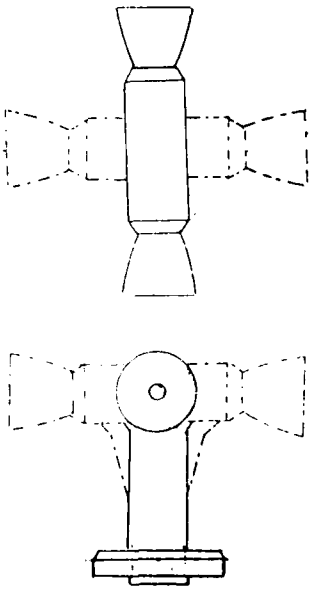

Figure 25. Two- and four-way fluidic diverter valves.

A conceptualized schematic drawing of an all fluidic KE projectile is shown in figure 26.

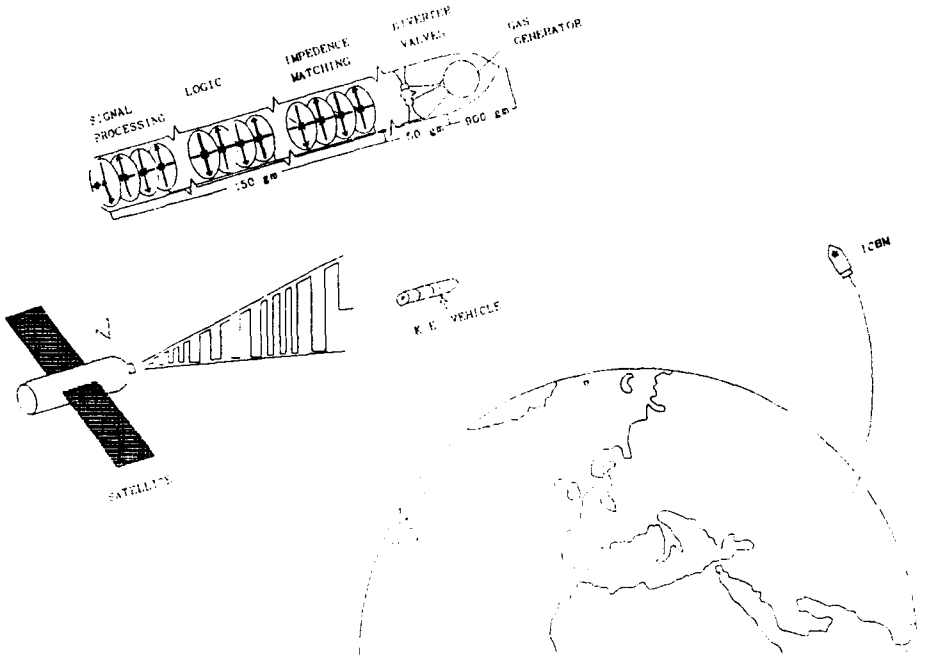

Figure 26. Schematic of an all-fluidic KEW projectile concept.

In this idealized concept a hostile ICBM booster is acquired by an acquisition system on board a satellite and a fire control solution is determined. A KEW projectile is launched towards an anticipated intercept point while the booster position is still tracked by the satellite. Corrective commands are transmitted to the projectile by a coded laser beam. These commands are demodulated in the opto-fluidic interface and converted into pressure signals that drive the diverter/thrusters which then steer the projectile to an intercept. If sufficient accuracy is not possible with the satellite tracking mechanism, then a seeker on the projectile can acquire the booster and can also command the fluidic system for a terminal homing solution.

4.1 Fluidic Flow Diverter Operation

A basic cross-section view showing the location and names of components used in a fluidic flow diverter is shown in figure 27. A diverter is comprised of a supply nozzle, receiver, four outlet diffusers, flow divider, four vortex amplifiers, cross-over bleed channels, four control ports and four opposing thruster nozzles.

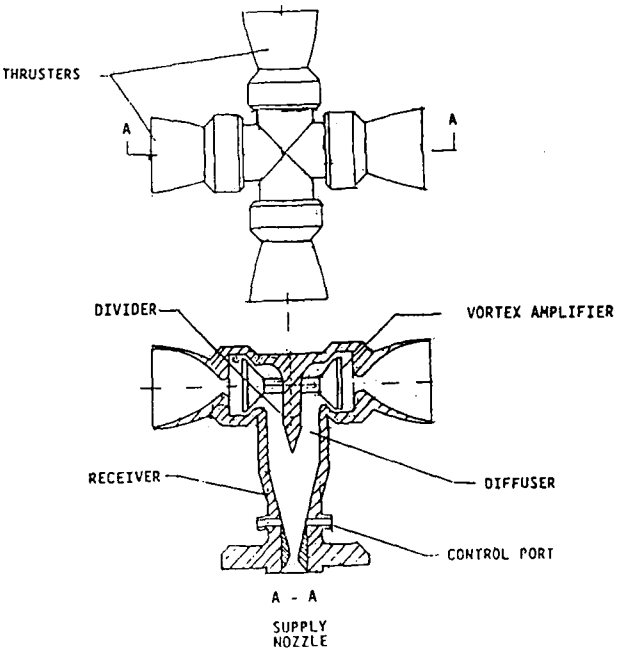

Figure 27. A fluidic diverter valve.

Operation of a fluidic diverter valve is illustrated in figure 28.

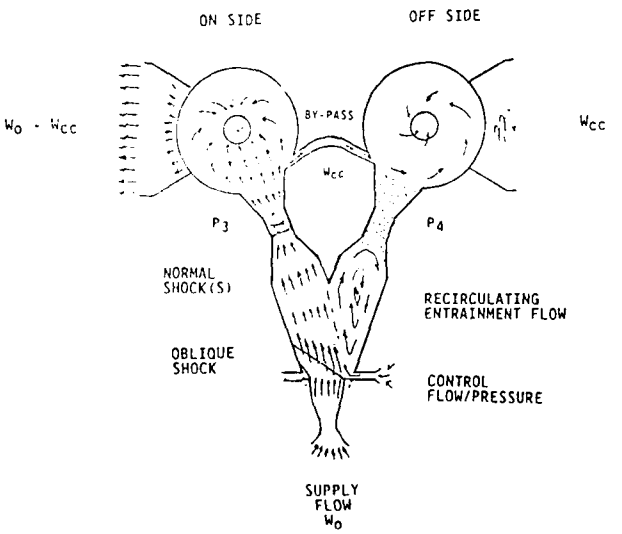

Figure 28. Operation of a fluidic gas diverter valve.

A solid propellant gas generator provides a constant flow rate of thruster gas. The gas enters the diverter through the supply nozzle at near-stagnation conditions. The gas is accelerated to supersonic velocities and leaves the nozzle in the form of a supersonic jet. The jet changes direction across an oblique shock wave and attaches to a side wall due to a resultant differential pressure force that is created by the entrainment characteristics of the jet. The jet flows along the wall to the diffuser where it is decelerated, recompressed across a normal shock wave and enters one of the four vortex amplifiers.

The vortex amplifiers perform two functions. First, they allow the propellant flow to pass easily through the vortex chamber to the outlet thruster when no vortex is generated. Second, they provide the means to isolate the internal nozzle jet flow from the external ambient environment. This occurs when a small portion of the jet flow is bled off through the bypass channel and used to pressurize the other vortex amplifier chambers as shown in figure 28. Because the bleed flow enters the chambers tangentially a vortex is produced in each one. The resultant action of the vortex creates centrifugal pressure forces that seal off the three non-flowing channels. The pressure forces essentially maintain the pressure in these three channels at the free stream static pressure in the jet stream at the jet boundary. The flow that produces the vortex then exits the vortex chamber through the chamber outlet and leaves the valve through the opposing outlet thrusters thus creating a small counter thrust.

The flow needed to produce a vortex in the amplifiers is dependent upon the static pressure in the non-flowing legs of the diverter and the physical design of the vortex chamber, bleed port and inlet geometry. The control flow rate needed is relatively low because of the high differential pressure between the pressure recovered in the flowing leg of the diverter and the static pressure in the non-flowing legs.

The valve supply flow is switched from one outlet to another by raising the pressure in the boundary layer between the attached jet flow and the wall of the receiver. This pressure rise can be produced by fluid injection (as would be the case with the valve actuated by a fluidic controller), tab insertion or electrical spark discharge. By raising the pressure in the boundary layer an adverse gradient is developed which causes the attached supersonic flow to separate. The mechanism of supersonic flow separation has been found to be dependent on Mach number, and gas properties at the point where separation begins to occur.

Fluidic diverters can be assembled into circuits that use multiple amplifying stages in order to reduce the power required to produce flow switching. The amplifiers are staged in such a way that the output of one stage becomes the input control to the

next. If the power (or flow) gain of an individual stage is known the total gain becomes equal to the gain per stage raised to the nth power where n is equal to the number of stages. A fluid amplifier typically operates with a flow gain equal to approximately 10. This implies that the flow required to actuate three stages in series is equal to 1/1000th of the total flow rate through the three stages. This results in a 1000:1 reduction in the power required for actuation.

As mentioned previously, other methods for actuating a fluidic diverter are tab insertion and spark discharge. In the tab insertion technique a small cylindrical cylinder is inserted into the boundary layer between the attached jet flow and the wall of the diffuser. This can be accomplished mechanically or with a fast-acting solenoid. The presence of the bluff body in the stream creates a disturbance in the supersonic stream boundary layer which destroys the normal shock structure and causes the stream to separate from the wall and switch over to the opposite side of the diverter. Although the resulting shock structure is very complex the effect has been demonstrated by experiments[12] and found to provide an effective method for actuating a diverter.

In the spark discharge technique a set of electrodes are mounted in the wall of the diffuser. The electrodes are used to release thermal energy into the stream as it passes through the outlet diffuser. The released energy destroys the natural normal shock structure and as a result makes the flow seek a more stable flow condition on the opposite side of the receiver. Spark discharge techniques could most effectively be used in conjunction with staged amplifiers in order to significantly reduce the amount of electrical power required to produce the flow diversion effect.

When no net thrust or control effort is desired, the fluidic diverter can be operated in a balanced output mode. In this operating mode the jet flow is expanded into the diverter and forced to attach symmetrically to all four walls downstream in the diverter receiver section. An illustration of a valve operating in the balanced output mode is shown in figure 29.

One of the principle advantages in using a fluidic type diverter in a high flow application is that the valve hardware can be housed inside the gas generator to save space, reduce valve wall thickness and to allow safe operation at very high gas generator pressures. Such a valve could be actuated with low power signals supplied externally through tubes leading through the walls of the diverter. A conceptual drawing illustrating the use of a multistage fluidic diverter in a high flow application is contained in figure 30.

---

[12] Fix, John, "Flueric Altitude Insensitive Thruster," ASME paper 69-WA/Flcs-XX, presented at the 1969 ASME Winter Annual Meeting.

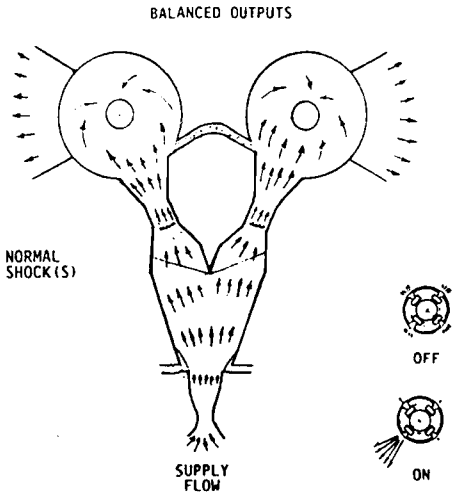

Figure 29. Fluidic diverter valve operation in a balanced mode.

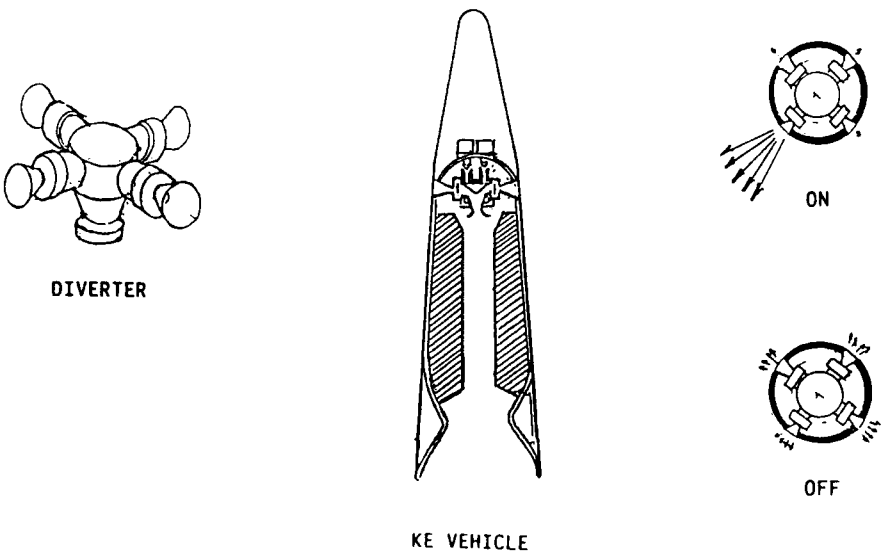

Figure 30. Valve concept for use inside gas generator.

4.2 Fluidic Flow Diverter Analysis

Several independent processes must be combined in order to insure efficient operation of a fluidic diverter. First, the supply nozzle must accelerate the high pressure propellant flow to supersonic velocity with very small losses. Second, the pressure in the off leg must be made equal to the free stream static pressure at the jet boundary in order to assure low leakage and stable attachment of the jet. Third, the flow entering the diffuser must be decelerated efficiently in order to optimize pressure recovery. Fourth, the control flow must generate the required pressure to produce separation and flow diversion to the opposite outlet. Lastly the vortex amplifier must operate with maximum turndown in order to reduce flow leakage and ensure optimum efficiency.

In the following sections each independent process is discussed separately and in conjunction with its operation in a diverter. Figure 31 shows a diagram of a generic diverter labelled with the parameters of interest.

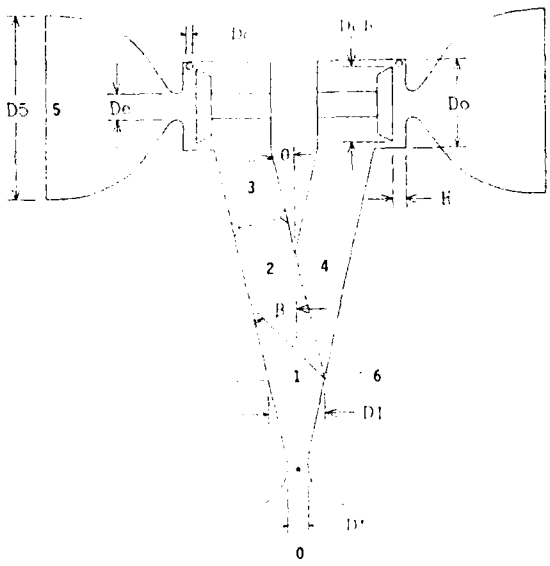

Figure 31. Nomenclature diagram of a diverter.

Supply Nozzle

The principal purpose of the supply nozzle is to reduce static pressure by accelerating the inlet flow to supersonic velocities. Flow enters the throat of the supply nozzle from the gas generator and is expanded supersonically to the desired Mach number (M_1) at the exit plane of the nozzle. The exit-to-throat area ratio

required to obtain the desired exit velocity is determined by the isentropic compressible flow relationship:

$$\frac{A_1}{A_*} = \frac{1}{M_1}\left[\frac{1 + [(k-1)/2]\ M_1^2}{(k+1)/2}\right]^{(k+1)/2(k-1)} \quad \ldots\ldots\ldots\ldots \quad (7)$$

where k is the ratio of specific heats

Figure 32 presents the results of computations using eq.7 that demonstrate that area ratio increases with increasing Mach number. For constant k (i.e. k = 1.2) , the throat-area-to-supply-exit-area ratio (A_*/A_1) increases exponentially. This has a significant impact on diverter size because diverters designed to operate at higher Mach numbers will be substantially larger than those that operate at lower Mach numbers.

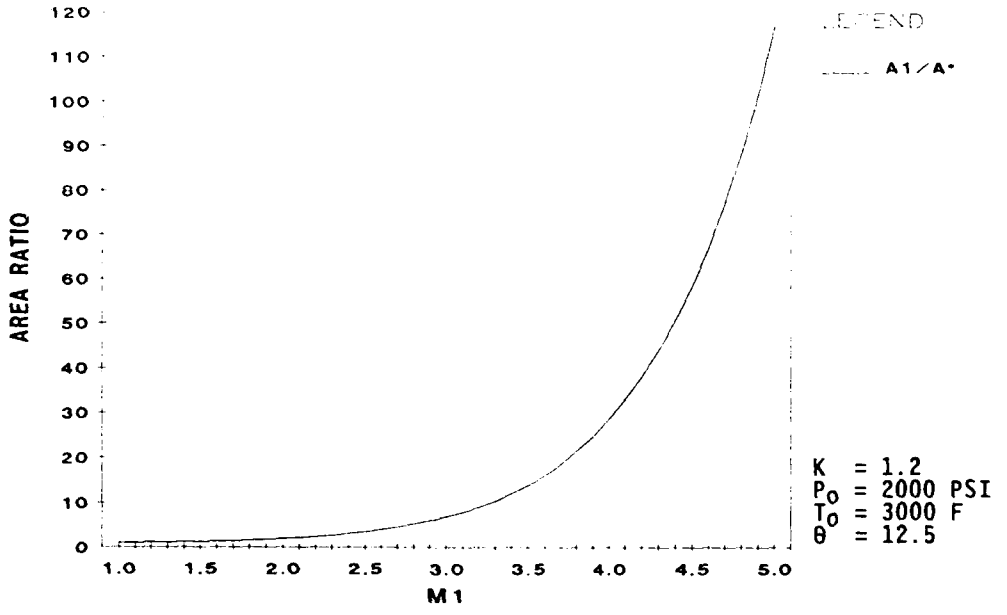

Figure 32. Computed values of A_1/A_* versus M_1

The supply nozzle throat area and gas properties govern the thrust and mass flow rate delivered by the reaction jets. The throat area of the supply nozzle is approximated by the maximum thrust equation, eq. 8, for the desired thrust, T, and gas properties at the inlet and exit plane of the nozzle. Once the throat area is determined, it follows that the mass flow rate W

is obtained from equation 9, and the nozzle exit area A_1, from equation 10.

$$A_* = T / P_0 \; k \left[\frac{2}{k-1} \left[\frac{2}{k+1} \right]^{\frac{(k+1)}{(k-1)}} \left[1 - \left[\frac{P_a}{P_0} \right]^{\frac{(k-1)}{k}} \right] \right]^{.5} \quad .. \quad (8)$$

$$W = \frac{P_0 \; A_*}{\sqrt{R \; T_0}} \sqrt{k} \left[\frac{2}{k+1} \right]^{(k+1)/2(k-1)} \quad ..... \quad (9)$$

$$A_1 = \frac{A_1}{A_*} A_* \quad ..... \quad (10)$$

In addition, the exit pressure of the supply nozzle can be readily calculated for any given nozzle exit Mach number by using the isentropic relationship:

$$\frac{P_1}{P_0} = \left[\frac{1 + [(k-1)/2] \; M_0^2}{1 + [(k-1)/2] \; M_1^2} \right]^{k/(k-1)} \quad ..... \quad (11)$$

Figure 33 shows that P_1 decreases monotonically with increasing M_1 in accordance with equation 11.

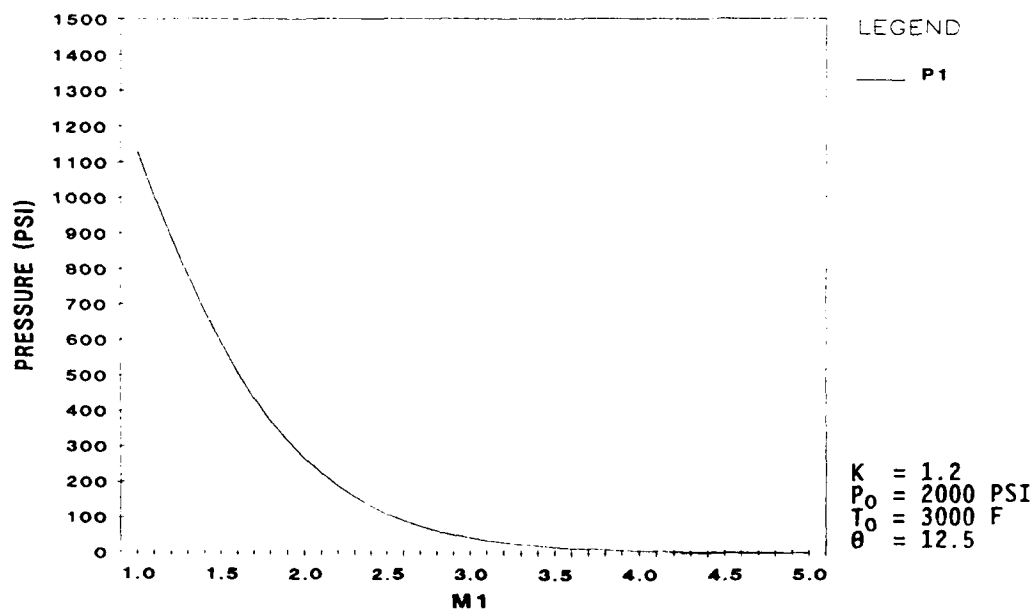

Figure 33. Exit pressure P_1 versus M_1

Diverter Chamber

The jet stream exiting the supply nozzle enters the supersonic diverter chamber where it is directed to one of the diffuser legs by a control pressure. The control, or separation pressure impinges on the jet from one side causing the jet to deflect. The deflected jet attaches to the opposing side and enters the corresponding diffuser.

The actual flow diversion process in a supersonic diverter depends upon the ability to create an adverse pressure gradient in the boundary layer between the attached supersonic jet flow and the wall of the valve. The separation of supersonic turbulent boundary layers has been studied by Morgan[13] and others who found that, in general, the ratio between the pressure in the boundary layer (P_6), required for switching, to the local free stream pressure where flow separation takes place (P_1) is a function of Mach number and may be obtained from equation 12.

$$\frac{P_6}{P_1} = \left[1 + \frac{.225\ k\ M_1^2}{1 + (k-1)/2\ M_1^2} \right] \left[1 + \frac{.18\ k \sqrt{M_1^2 - 1}}{[1 + .28\ (k-1)\ M_1^2]\ 1.2\ (P_6/P_1 - 1)} \right] \quad \ldots\ldots\ldots \quad (12)$$

Figure 34 shows the separation pressure for two propellants that produce gasses of different specific heat ratios. The curves indicate that the pressure required to initiate separation is between two to three times the static pressure at the exit plane of the supply nozzle for $k = 1.2$ and $2 \leq M_1 \leq 4$.

The control flow rate required to produce flow separation in a nozzle has been shown by Mager[14] and others to be on the order of only a few percent of the total nozzle flow. In early diverter experiments conducted by Holmes[15] it was shown that the supply jet in a diverter could be separated and deflected completely to

---

[13] Morgan, E.J., "An Analysis of Gaseous Secondary Injection into Rocket Nozzles," American Rocket Society, Solid Propellant Rocket Conference paper no. 2335-62, 1962.

[14] Mager, A., "On the Model of the Free, Shock-Separated, Turbulent Boundary Layer," J. of the Aeronautical Sciences, pp 181-184, Feb 1956.

[15] Holmes, A. B., "Supersonic Fluid Amplification with Various Expansion Ratio Nozzles," Proceedings of the 1st Fluid Amplification Symposium, 1964.

the opposite wall of a receiver with a control flow as little as 2 - 3 percent of the supply flow. This would imply that any valve placed upstream of the control nozzle or any fluid amplifier used for supplying the control flow must be sized to deliver a flow rate equal to approximately 2 - 3 percent of the total supply flow at a pressure equal to approximately 2.5 times the local static pressure at the control nozzle outlet.

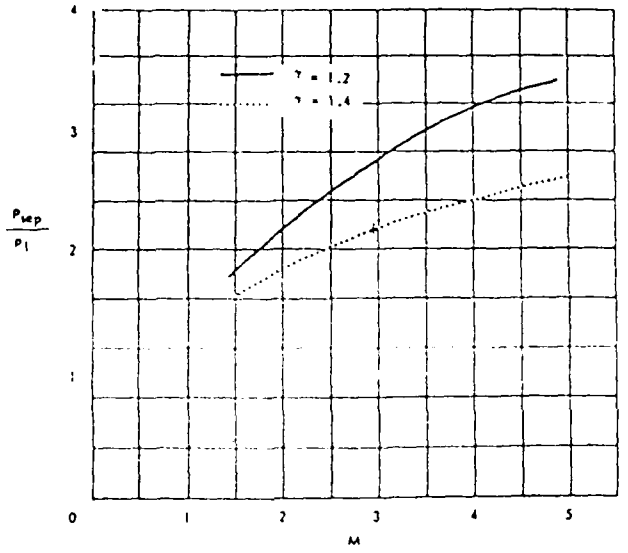

Figure 34. Separation pressure ratio, P_6/P_1, versus M_1

Once the jet has been intentionally detached from one side of the diverter it will automatically reattach itself to the opposing chamber wall due to negative pressure on that wall due to the restriction of entrained flow on that side, a phenomenon that is known as the Coanda effect. The Coanda effect and separation pressure, however, are incapable of maintaining the flow if the pressure in the off-leg is too low. If the off-leg pressure is low enough, a portion of the jet stream will expand into the off-leg resulting in poor efficiency of the guidance propulsion system. To avoid this problem vortex valves are placed at the end of each diffuser. The vortex valves maintain the off-leg pressure at the jet free boundary static pressure thereby insuring that no main jet flow leaks down the off-leg.

The static pressure of the jet in the diverter section is dependent on the oblique shock angle. When a supersonic jet exits the supply nozzle it is deflected by the control pressure as discussed earlier. The diverter chamber walls and diffuser present a physical boundary to the jet stream which dictate the deflection angle θ. The deflection angle is measured from the

supply nozzle axis. Given the deflection angle, the angle of the oblique shock, β (also measured from the supply nozzle axis), may be calculated from equation 13.

$$\tan \Theta = \frac{2}{\tan \beta} \frac{M_1^2 \sin^2\beta - 1}{M_1^2 (k+\cos^2\beta) + 2} \quad \ldots\ldots\ldots\ldots\ldots\ldots \quad (13)$$

After the shock angle is determined, the static pressure in the deflected jet (P_2) is found by calculating the pressure ratio across the oblique shock from eq. 14.

$$\frac{P_2}{P_1} = \frac{2k}{k+1} M_1^2 \sin^2\beta - \frac{k-1}{k+1} \quad \ldots\ldots\ldots\ldots\ldots\ldots\ldots \quad (14)$$

Figure 35 shows the results of computations comparing P_1 and P_2 as M_1 is increased from one to five for $k = 1.2$ and $\Theta = 12.5°$.

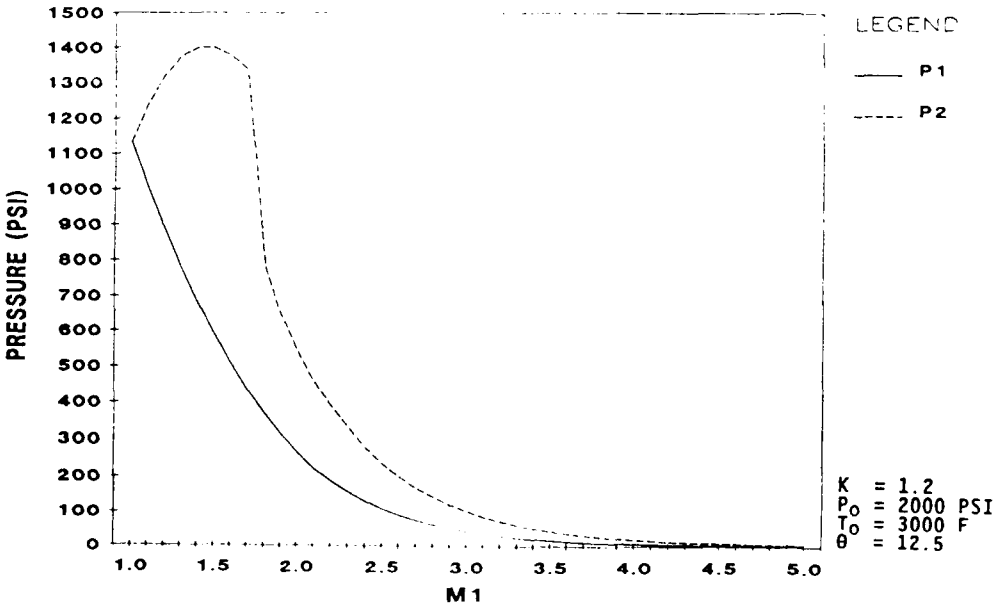

Figure 35. Relationship between the pressure before the shock and the pressure in the shock versus M_1.

At lower supersonic velocities ($1.0 \leq M_1 \leq 1.5$) the energy of the jet is insufficient to remain supersonic after being redirected in the diverter chamber, thus the flow goes subsonic and generates undesirably high static pressures at the free boundary. At higher Mach numbers ($M_1 > 1.5$), however, the flow is not decelerated enough to become subsonic, instead a strong oblique shock exists and P_2 decreases with increasing M_1.

The Mach number downstream of the oblique shock, M_2 is determined by equation 15.

$$M_2 = \left[\frac{2 + (k-1)\ M_1^2}{2\ k\ M_1^2\ \sin^2\beta - (k-1)} + \frac{2\ M_1^2\ \cos^2\beta}{2 + (k-1)\ M_1^2\ \sin^2\beta} \right]^{.5} \quad .. \quad (15)$$

Jet Deflection Angle Considerations

The angle through which the supply jet is deflected is dependent on the physical boundary of the diverter chamber walls and diffusers. There are two counteracting issues to be considered when establishing the deflection angle θ for a diverter. The first consideration is that of diverter efficiency. Reducing deflection angle will decrease the off-leg pressure and increase the on-leg pressure recovery hence the thrust efficiency will be increased because less flow that develops counter thrust is bled off to shut down the off-leg. This is illustrated in figure 36 which shows the computed thrust efficiency as a function of diverter divergence, or deflection, angle.

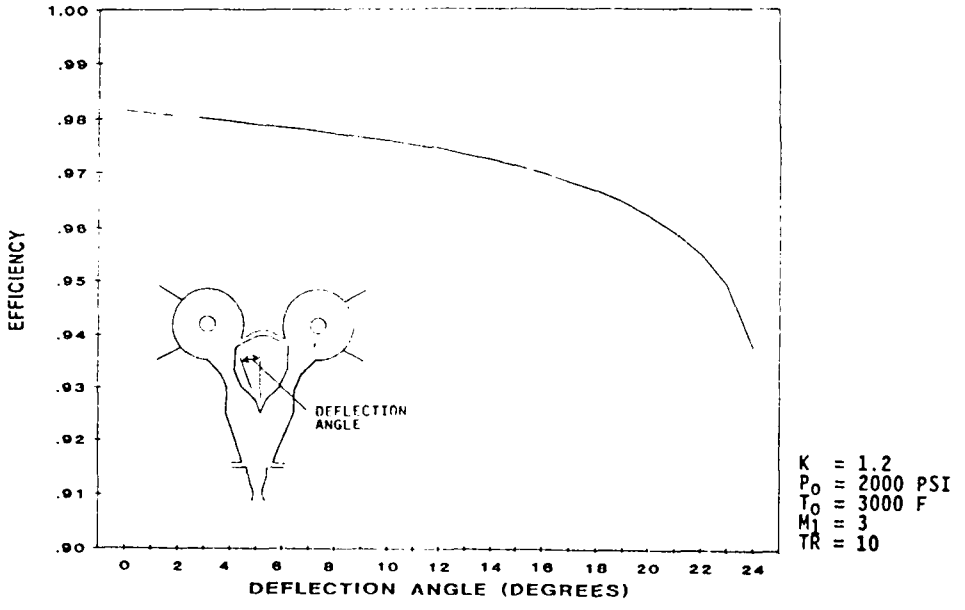

Figure 36. Thrust efficiency versus deflection angle.

On the other hand, reducing the jet flow deflection angle by reducing the wall divergence angle in the receiver will require that the divider be placed further downstream in order to accommodate the desired width of diffusers. This results in a longer distance for the free boundary between the nozzle and

divider which will result in the jet having to travel a longer distance before reaching the diffuser. As a result, the jet will have spread significantly due to turbulent mixing which in turn would cause leakage in to the off-leg, and a reduction in pressure recovery.

Diffuser Design

The diffuser section of the diverter converts the supersonic, low pressure gas flow of the diverter chamber into a subsonic, high pressure gas flow that is required for the vortex valves to operate. Once the stream has entered a diffuser, the stream velocity is reduced from supersonic to subsonic velocity across a normal shock. This produces the recovered pressure necessary to obtain a high on-leg to off-leg pressure ratio to turn the off-leg vortex valve off. Under ideal conditions the velocity distribution across the entrance of the diffuser is uniform and the pressure recovered across the normal shock can be calculated from the following normal shock and isentropic relationships:

$$\frac{P_3}{P_2} = \frac{(1 + k\ M_2{}^2)}{(1 + k\ M_3{}^2)} \qquad (16)$$

$$P_{t3} = P_3 \left[1 + \frac{k - 1}{2} M_3{}^2 \right]^{k/(k-1)} \qquad (17)$$

$$M_3 = \left[\frac{(k-1)\ M_2{}^2 + 2}{2\ k\ M_2{}^2 - (k-1)} \right]^{.5} \qquad (18)$$

In practice inlet losses caused by asymmetric velocity distributions, boundary layer growth, and other effects tend to reduce the pressure below that which is calculated using the above relationships.

Figure 37 shows the calculated results for the Mach number after the oblique shock, M_2, and after the normal shock in the diffuser, M_3 as a function of the nozzle Mach number, M_1, for k = 1.2. This figure clearly shows how M_2 is subsonic for $1.0 \leq M_1 \leq 1.5$ and then increases at the same rate as M_1 for $M_1 < 1.5$. M_3 decreases as M_1 increases.

In general, and especially at higher supply nozzle diffuser entrance Mach numbers, it is desirable to pass the jet flow through a slightly convergent passage before recompressing it through a normal shock wave. The reason for doing this is that by slowing the fluid velocity, recompression occurs at a lower Mach number and therefore the pressure recovered will be higher. The design of an efficient diffuser is one of the most important

factors governing the design of an efficient diverter. This convergence geometrical parameter has to be determined experimentally to insure maximum efficiency.

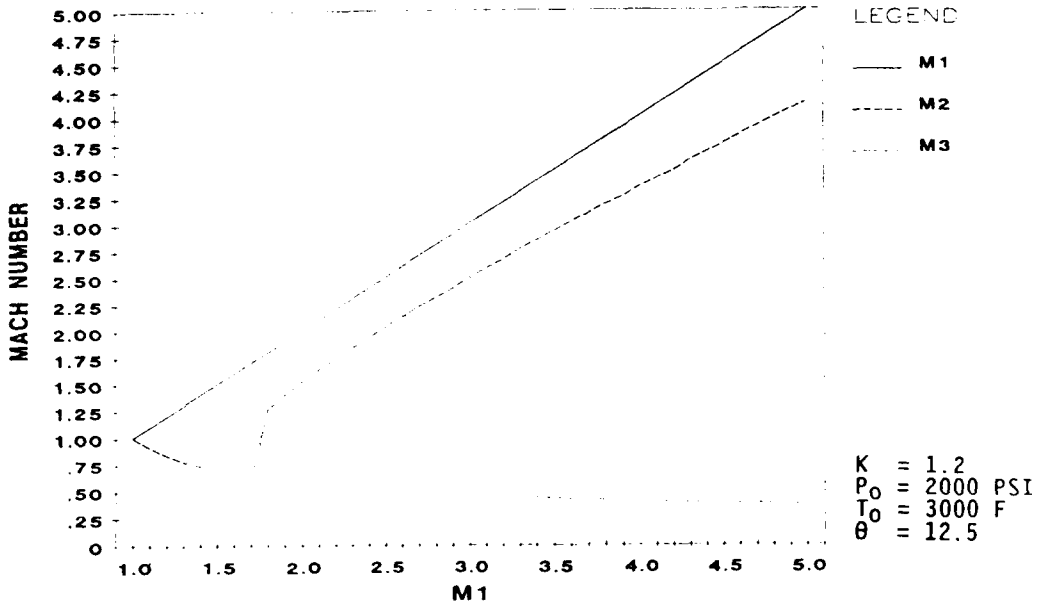

Figure 37. Mach numbers in valve versus M_1

Loading also has a strong effect on the pressure recovered in any diffuser of this type. Loading in this case refers to the resistance to flow that the combined vortex chamber and outlet nozzle present to the flow. This parameter is usually represented in terms of a discharge coefficient and nozzle outlet area. Although the load resistance can be calculated with fair accuracy using orifice equations and published discharge coefficients, a change in a few percent above or below the optimum value changes the position of the normal shock in the diffuser, which directly affects performance. In a worst case scenario, this can move the shock through the inlet causing leakage into the off-side channel, and/or cause jet instabilities and random switching of the jet.

Vortex Amplifiers

A conceptual drawing illustrating the features of a vortex amplifier are shown in figure 38. The vortex amplifier consists of a cylindrical chamber that is enclosed on both ends by flat plates. As shown in figure 38 there are two inlet ports and one outlet port. The two inlets are the supply and control ports which enter the chamber radially and tangentially respectively. The outlet port is central to one of the end plates and exits the chamber axially.

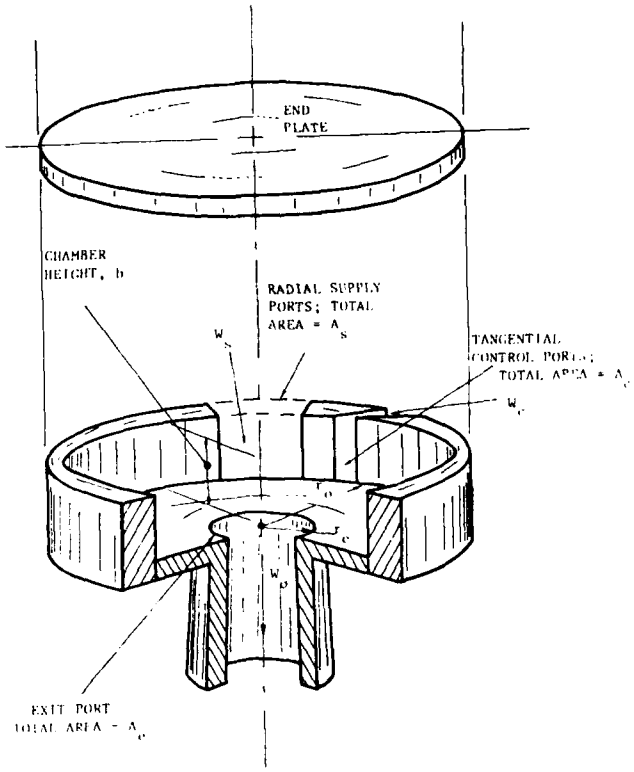

Figure 38. Conceptual illustration of a vortex amplifier.

The purpose of the vortex valve is to maintain the pressure in the "off-leg" so that the jet is not sucked out of the wrong thruster into the vacuum of space. Each diffuser leg has a vortex valve at the end of it and the control ports of each of the valves are connected to one another.

Gas enters the vortex valve supply port from the "on-leg" diffuser, and in the absence of a vortex the flow proceeds radially through the chamber and exits through the central outlet continuing out through the thruster nozzle and produces thrust. A small amount of flow bleeds off to the other vortex valves. In this mode of operation the flow rate is at its maximum level and the vortex valve is considered to be fully open. When the stream is diverted into another diffuser, however, bleed control flow from the now on leg is injected through the control port closing the valve. The control flow enters the vortex chamber tangentially creating a "free" vortex. In a "free" vortex, conservation of angular momentum requires that the tangential velocity of the fluid increase with decreasing radius such that the tangential velocity, V_t, is equal to:

$$V_t = V_{to} (r_o/r)^n \quad \ldots\ldots\ldots\ldots\ldots\ldots\ldots\ldots\ldots\ldots\ldots\ldots\ldots\ldots \quad (19)$$

where V_{to} is the tangential velocity at the outer chamber radius, r_o, r is the chamber radius at which the velocity is measured, and n is the vortex exponent which ranges between -1 and 1, depending upon the viscosity of the fluid.

The corresponding differential pressure forces that are produced between the slower (higher pressure) fluid at the outer edge of the vortex chamber and the faster moving (lower pressure) fluid near the center of the vortex chamber can be expressed as:

$$dP = (\rho V_t^2 \, dr) / r \quad \ldots\ldots\ldots\ldots\ldots\ldots\ldots\ldots\ldots\ldots \quad (20)$$

where o is the fluid mass density and dP is the differential pressure across a differential radial element dr. It should be noted that in a diverter valve the by-pass bleed flow represents the only flow that passes through the vortex flow field produced in the chamber.

Specific procedures for establishing the operating characteristics of a vortex valve have been developed by numerous experimenters and have been cataloged by Wormley[16]. Basically the results of this work have shown that the throttling characteristics of a vortex valve are a function of only two non-dimensional geometric ratios, A_c/A_e, the ratio of control channel area to exit area and r_e/r_o, the ratio of exit orifice radius to vortex chamber radius, within specified bounds for A_s/A_e, the ratio of supply port area to exit area, and h/r_e, the ratio of vortex chamber height to exit orifice radius. The supply area, A_s, has a negligible effect on vortex valve characteristics if $A_s/A_e \geq 3.0$ and height h has a negligible effect if $h/r_e \geq 2$. Since size is a major consideration, the minimum possible values ($A_s/A_e = 3$ and $h/r_e = 2$) have been selected.

The data shown in figure 39 is used to determine A_c/A_e and r_e/r_o based on the flow parameters $P_{cc} = Pc/Ps = P_{t3}/P_4$ and $W_{cc} = W_c/W_s = 1/TR$. P_c/P_s is the control pressure to supply pressure ratio.

P_c is equal to the recovered (total or stagnation) pressure after the normal shock of the on-leg. This pressure is the driving force responsible for closing the off-leg vortex valve and isolating the off-leg pressure from ambient. P_s, the off-leg supply pressure is equal to the static pressure of the jet stream at the free boundary (pressure downstream of oblique shock). W_c and W_s are control and supply mass flow rates respectively, and W_s/W_c equals the turndown ratio TR. The maximum possible turndown ratio (minimum W_{cc}) from figure 39 is selected to maximize mass flow efficiency. Having chosen TR to get W_{cc} and by calculating the supply and control pressures as shown earlier, the A_c/A_e and r_e/r_o ratios can be determined from figure 39.

---

[16] Wormley, D.N., "A Review of Vortex Diode and Triode Static and Dynamic Design Techniques," Proceedings of the Fluidic State-of-the-Art Symposium, Vol 1, 1974.

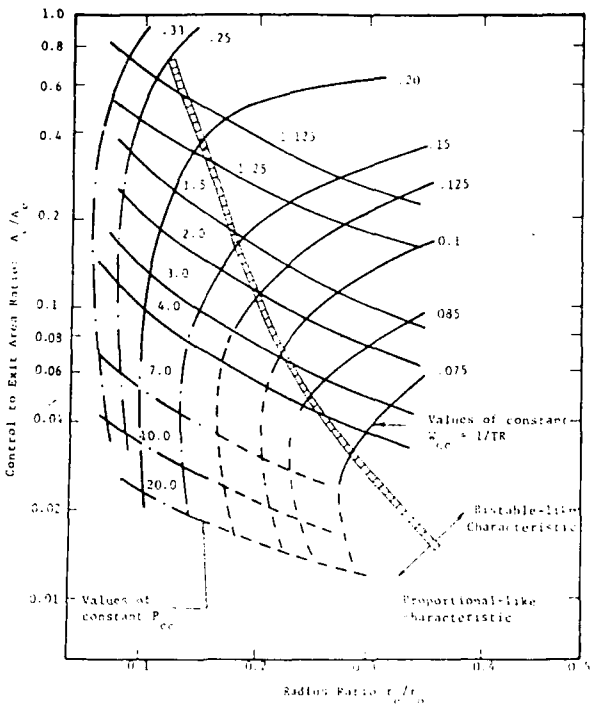

Figure 39. Vortex amplifier design parameters.

The vortex valve dimensions are completely derived from the ratios A_s/A_e, h/r_e, A_c/A_e and r_e/r_o. Examining these ratios it is evident that the vortex valve dimensions are based fundamentally on the exit area of the valve. The exit area is critical to more than the peripheral valve dimensions, but is also critical to establishing the choked flow and high stagnation (control) pressures required. The exit area is determined based on the quadratic relationship:

$$A_e = W / C_d \sqrt{2 \rho (P_{t3} - P_5)} \quad \ldots\ldots\ldots\ldots\ldots\ldots\ldots\ldots \quad (21)$$

where C_d is the discharge coefficient.

Efficiency

In the diverter valve the turn-down ratio and the ratio between the on-leg and off-leg pressures determines the operating efficiency because the amount of bleed flow required to isolate the "off-side" from the vacuum environment determines the amount of counter thrust acting against the primary thrust as well as the amount of flow not available in the main stream to act as thrust. This is because the bleed flow produces a reaction force which opposes the primary force produced at the primary output. The relative amount of control flow required is a function of the pressure in the non-flowing side of the diverter and the geometry of the vortex valve.

Upon leaving the vortex valve the two gas streams representing the primary flow and the bypass flow are expanded to exit velocities that are equal in each of the opposing nozzles. This means that the ability of the valve to produce thrust forces efficiently is determined by the relative amount of fluid discharged through each outlet. The factor defining efficiency of a two-way valve is equal to:

$$\eta = (W - 2W_{cc}) / W \quad \ldots\ldots\ldots\ldots\ldots\ldots\ldots\ldots\ldots\ldots \quad (22)$$

and the equation describing the efficiency of a four-way valve is given as:

$$\eta = (W - 4W_{cc}) / W \quad \ldots\ldots\ldots\ldots\ldots\ldots\ldots\ldots\ldots\ldots \quad (23)$$

It should be noted that in comparing the efficiency of a two-way valve with that of a four-way valve that one four-way valve replaces two two-way valves and that the two-way valves consume twice the four-way valve system flow rate and as such can only approach 50-percent efficiency. Figure 40 shows the relative efficiency of each of the diverter valve systems. It can be easily seen that although the actual efficiency of a four way valve is somewhat lower because of the additional control flow required to isolate two additional outlet channels, the relative amount of propellant that is consumed in each system is half.

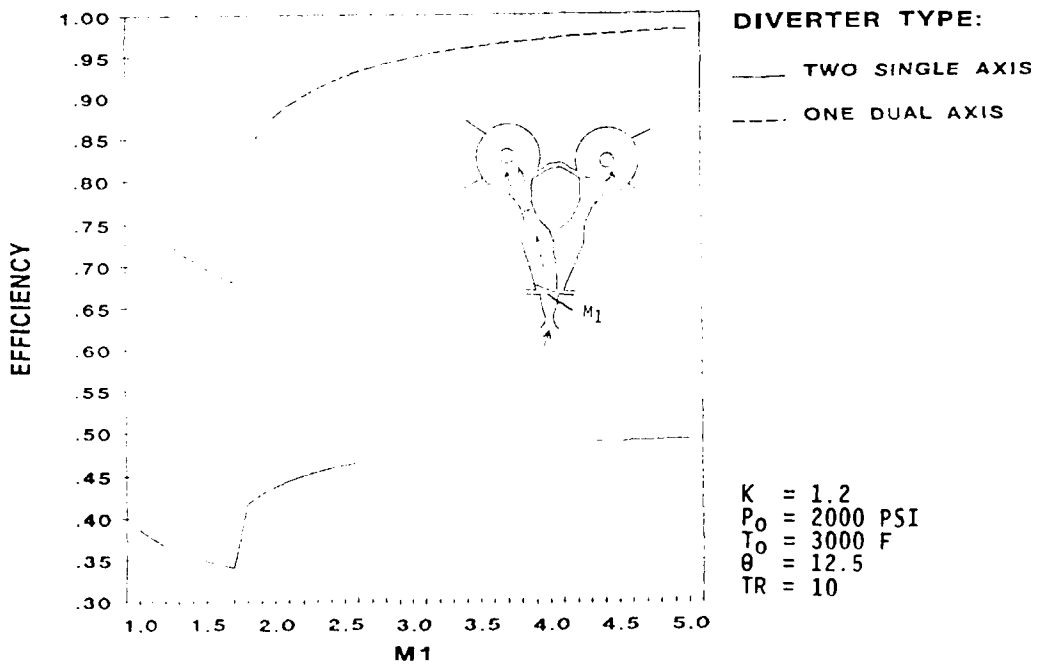

Figure 40. Comparison of the efficiency of two single-axis valves with one dual-axis valve.

Diverter Design Summary

In summary, Defense Research Technologies, Inc. has developed an efficient procedure for the design of supersonic diverters to control high energy propellant gasses that considers -

1. The effects of supply nozzle Mach number (Area ratio) on valve geometry and performance.

2. Pressure distributions along the flowing and non-flowing sides of a pressurized diverter operating over a range of supply nozzle Mach numbers.

3. The effects of supply nozzle Mach number, and vortex valve performance on recoverable impulse between the two opposing valve outlets.

4. The pressure levels required for producing flow separation and diversion over a range of supply nozzle Mach numbers.

5. The maximum attainable efficiency of supersonic hot gas diverters.

4.3 Preferred Diverter Design and Projected Performance

Theoretical investigations were conducted to obtain information for the design geometries of supersonic gas diverters which can be used in the diverters to produce high recoverable efficiencies. Calculations of nozzle area ratio, Mach number, oblique shock pressure recovery, diffuser pressure recovery, on-side and off-side pressure ratios and critical vortex valve dimensional relationships were obtained over a supply nozzle Mach number range of 2.0 to 5.0 using air ($k = 1.4$) and a propellant ($k = 1.2$).

The influence that the various parameters have on diverter performance was determined by the theoretical analysis as implemented in a computer model. The program was exercised to determine the effects of flow velocity, supply gas properties and certain dimensions on the diverter size and efficiency.

Diverter size and efficiency are the most critical design parameters. The diverter needs to be as small as possible and work as efficiently as possible to reduce power requirements. The starting place for designing the diverter guidance propulsion system is the gas generator. Early results of the analysis showed that it was best to use a propellant that burns as hot as possible to reduce mass flow requirements and to burn at as high a pressure as possible to reduce size.

In addition, the propellant should have as high a gas constant as possible. An increase of 40 percent will reduce mass flow

rate requirements by 15 percent. Varying the specific heat ratio has various effects on diverter operation. By reducing k from 1.4 to 1.2 and keeping all other properties constant (P_o = 2000 psi, T_o = 3000°F and R = 53.3 $ft \cdot lb_f/lb_m \cdot °R$) efficiency increases by six percent but supply nozzle exit area increases by 28 percent. Although the supply nozzle is larger, the vortex valve decreases in size by 2.5 percent. Another advantage to a lower specific heat ratio is a net reduction in separation pressure by 12.4 percent. Figure 34 showed P_{sep}/P_1 to be higher for k = 1.2 than for k = 1.4, however, P_1 is actually much smaller for k = 1.2 so that the separation pressure required for k = 1.2 is in fact less than that for k = 1.4.

Given the above supply gas considerations, the temperature, pressure, gas constant, and specific heat ratio shown in Table 6 were selected. The values chosen fall within the ranges normally specified for miniature hot gas valves.

Table 6. Baseline Supply Gas Properties

$k = 1.2$
$R = 53.34\ ft \cdot lb_f/lb_m \cdot °R$
$P_o = 2000$ psia
$T_o = 3000°F$

A parameter with a significant effect on valve size is the thrust requirement. Thrust and nozzle area have a one-to-one relationship. If the desired thrust is doubled the supply nozzle exit area, as well as all other cross-sectional areas, must be doubled to accommodate the new thrust. The overall size of the valve however will only increase by a factor of 1.414 for each doubling of thrust. A thrust of 10 lb_f was selected for analysis and design purposes because the corresponding flow requirements are obtainable at the Defense Research Technologies laboratory facility.

The Mach number at the supply nozzle exit plane is another design parameter that cross-sectional area, and hence overall size, is dependent on. Figure 32 showed that the area of the supply nozzle exit increases exponentially with increasing M_1. This suggests designing a diverter valve that operates at low Mach number.

Another parameter that is directly affected by the supply nozzle exit Mach number is separation pressure. The separation pressure required to deflect the primary jet is dependent on P_1 and M_1 as shown in figure 34. Since P_1 decreases with increasing Mach number due to jet expansion in the supply nozzle then P_6 (P_6 = P_{sep}) actually decreases with increasing M_1 as shown in figure 41. Therefore, a diverter which operates at higher Mach numbers requires less control pressure to deflect the primary jet.

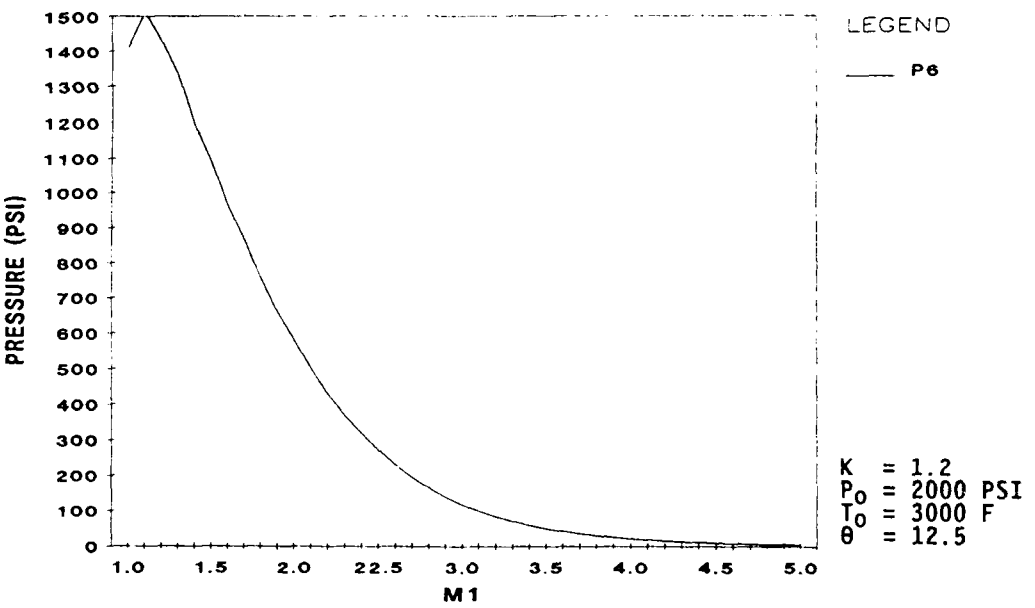

Figure 41. Separation Pressure Versus M_1

One other important issue to consider, when determining the diverter valve design as it pertains to Mach number, is thrust efficiency. As Mach number increases the jet edge pressure drops so that the off-leg pressure is reduced therefore requiring less bleed flow from the on-leg to shut off the off-leg vortex valve. Figure 42 shows a plot of thrust efficiency for a single-axis diverter system versus M_1.

Figure 42 also shows four curves representing performance with vortex valves with various turndown ratios. Efficiency not only increases by increasing Mach number but also by increasing turndown ratio. A turndown ratio of ten is selected for the vortex valve design because it provides exceptionally good efficiency and is the highest reasonably obtained turndown ratio.

The input parameters required by the computer program to perform the analysis as outlined in the theoretical analysis section are those given in Table 6 with the addition of an exit Mach number, $M_0 = 0$, thrust, T= 10 lb_f, deflection angle, $\theta = 12.5°$, turndown ratio, TR = 10, and nozzle Mach number, $M_1 = 3$. A supply nozzle exit Mach number of three was chosen as a first cut because this velocity provides high efficiency requiring a reasonable separation pressure all of which will fit in a package only one and one-half cubic inches small.

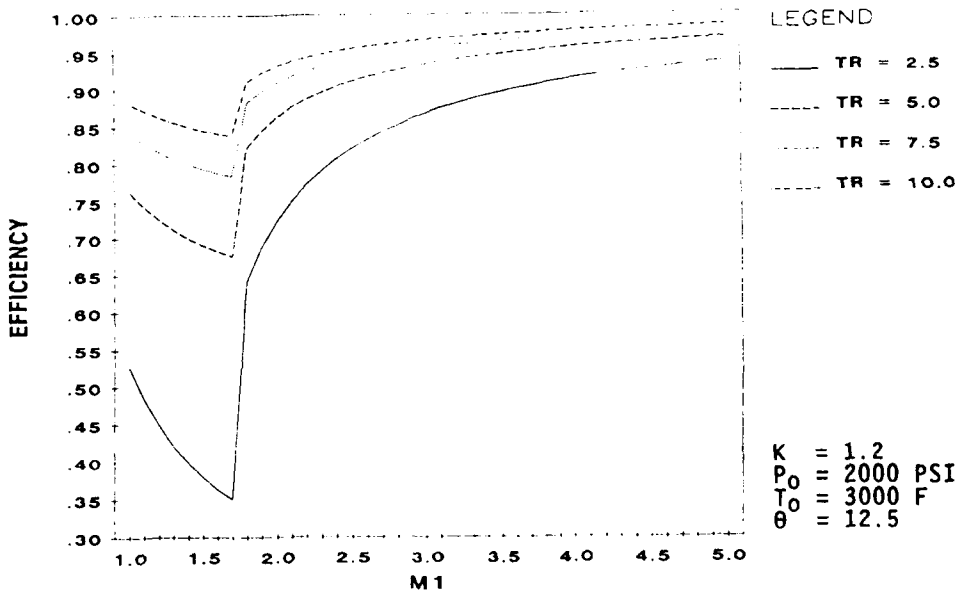

Figure 42. Efficiency Versus M_1

The final design output is shown in Table 7. This partial output includes flow velocities downstream of the oblique and normal shocks, mass flow rate, oblique shock angle, efficiency, pressures at six locations in the diverter, important vortex valve parameters, and the critical dimensions of the diverter valve. With these specifications an engineering drawing was generated.

Table 9. Diverter Valve Computed Design

OUTPUT:

M2 = 2.48678
M3 = .4701777
W = 3.811535E-02 lbm/sec
β = 30.26167 °
η = .9664707

Pressures:
P1 = 42.51167 psi
P2 = 102.1373 psi
P3 = 679.76 psi
Pt3 = 775.0563 psi
P4 = 102.1373 psi
Pt3/P4 = 7.588375
P5 = 0 psi
P6 = 116.907 psi
P6/P1 = 2.749999

Vortex Valve:
Ps = 102.1373 psi
Pcc = 775.0563 psi
PR = Pcc/Ps = 7.588375
Wm = 3.811535E-02 lbm/sec
Wcc = 6.389915E-04 lbm/sec
re/ro = .3
Ac/Ae = 1.676468E-02
As/Ae = 3
h/re = 2

Dimensions:
A* = 2.225419E-03 in²
A1 = .0149891 in²
A1/A* = 6.735405
As = 9.576192E-03 in²
Ac = 5.351392E-05 in²
Ae = 3.192064E-03 in²
A5 = .1596032 in²
A5/Ae = 50
H = .0637516 in
D* = 5.323055E-02 in
D1 = .1381474 in
Do = .2125053 in
Dcb = .1815646 in
Dc = 8.254456E-03 in
De = .0637516 in
D5 = .4507917 in

Figure 43 is the engineering drawing that has been developed from the computer simulation results presented in table 7.

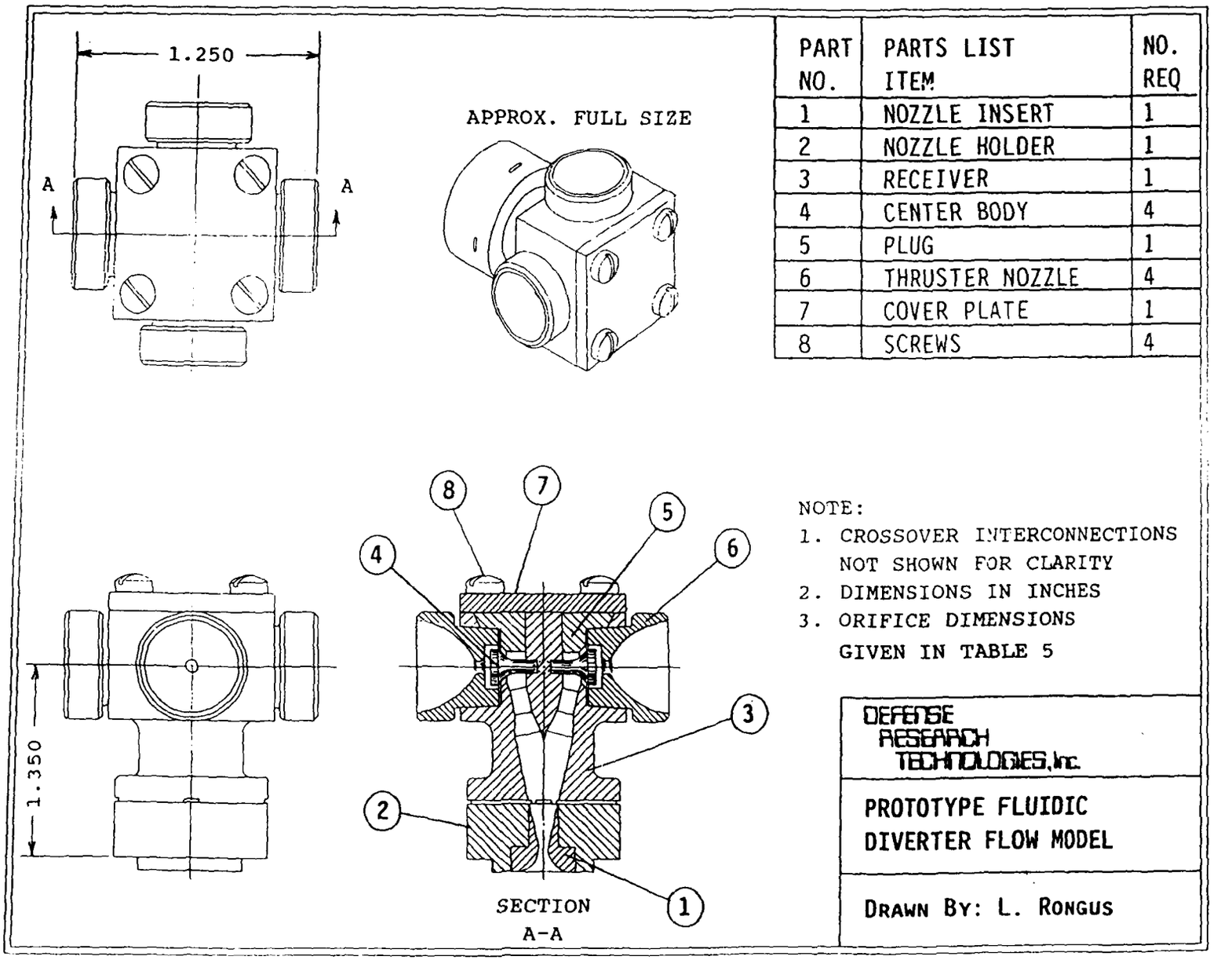

PART NO.	PARTS LIST ITEM	NO. REQ
1	NOZZLE INSERT	1
2	NOZZLE HOLDER	1
3	RECEIVER	1
4	CENTER BODY	4
5	PLUG	1
6	THRUSTER NOZZLE	4
7	COVER PLATE	1
8	SCREWS	4

Figure 43. Engineering drawing of the preferred valve.

5. MATERIALS

The fluidic control system as well as the fluidic diverters are not subject to the same restrictions that have plagued the development of KEW projectiles. In an attempt to reduce weight, conventional designs have been forced to use extremely high temperature burning propellants to maximize in I_{sp}, (specific impulse) and as a result have severely taxed materials capabilities. Parasitic weight is a perennial KEW problem. Having to carry around batteries, power supplies, gas bottles, mechanical valves, etc. has driven up the weight, but since these parasitic (e.g. they do not materially contribute to the kinetic energy lethal mechanism) are necessary for the operation of conventional systems they have had to be tolerated. By readjusting the conventional mind set to the consideration of an all-fluidic projectile it becomes clear that one may be able to deliver a 0.5 kg mass on target without having to consider esoteric propulsion systems or consequently esoteric materials. Graphite has already been discussed as a leading contender material for the signal processing, however the diverters will be handling warm or hot gasses and as such will have to be constructed to withstand at least 2000°F and possibly as high as 4000°F. Higher temperatures need only be considered when the fluidic diverters are being used in conjunction with otherwize conventional projectile designs. Table 8 shows a listing of materials suitable for the monolithic construction of fluidic laminations and diverter valve bodies.

Table 8. Refractory Construction Materials

Material	Melting Temperature	Specific Gravity	Oxidation Resistance
2-D Carbon-Carbon	>7000°F	2.0	Poor
3-D Carbon-Carbon	>7000°F	2.0	Poor
4-D Carbon-Carbon	>7000°F	2.0	Poor
ATJ Graphite	>7000°F	2.0	Poor
Pyrolytic Graphite	>7000°F	2.0	Poor
Graphnol	>7000°F	2.0	Poor
Poco Graphite	>7000°F	2.0	Poor
Tantalum	5400°F	16.6	Poor
Molybdenum	4700°F	10.2	Poor
Tungsten	>5400°F	19.3	Poor
Rhenium	5400°F	21.0	Poor
Iridium	4400°F	22.4	Fair >2000°F

Due to the poor oxidation resistance of all the construction materials it is necessary to coat them with thin layers of oxidation resistant materials. These generally do not have the same strength or shock resistance hence can only be used in thin layers. Table 9 shows a listing of suitable materials for

coating the inside passages of monolithic structures such as the diverter nozzle and interaction regions, to prevent oxidation of thin walled, lightweight metal structures.

Table 9. Refractory Coating Materials

Material	Melting Temperature	Specific Gravity	Oxidation Resistance
Silicon Carbide	>4600°F	3.2	Good <3000°F
Boron Carbide	4400°F	2.5	Good <2000°F
Zirconium Carbide	6200°F	6.6	Good <2000°F
Zirconium Diboride	5500°F	6.1	Good <2000°F
Hafnium Carbide	7000°F	12.7	Poor >1000°F
Magnesium Oxide	>5100°F	3.6	Good

Each of the coating materials are readily adaptable to the coating of fluidic format laminations or the intricate internal passages of the diverter. Manufacturing processes that are available are: CVD (chemical vapor deposition), APS (arc-plasma-spray), HIP (hot isostatic pressing), or PVD (physical vapor deposition).

6. PHASE I SUMMARY AND CONCLUSIONS

The Phase I study of the feasibility of developing fluidic guidance for KEW projectiles has demonstrated, in brassboard hardware the capability to -

* Detect and process tactically realistic laser guidance beam fluences of less than 1 W/cm^2.

* Develop multiple (four) useful command signals operating off a guidance law reasonable 4000 Hz carrier with a response time of approximately 2 ms.

* Develop sufficient command flow rates to directly drive a fluidic supersonic diverter.

* Perform the required processing with an extremely modest expenditure of power (320 mW) that may be available as bleed from the propulsion system thereby not requiring a separate power source.

In addition, engineering estimates based on reasonable manufacturing processes and design considerations for a diverter valve have shown the feasibility of a KEW projectile guidance system with the following characteristics -

* Thrust delivered from a single, continuously burning solid propellant gas generator of 10 lbs with a thrust efficiency in excess of 93-percent.

* Diverter size of less than 25 mm length and 30 mm overall diameter.

* Overall mass including both the signal processor and the diverter of less than 500 gm.

* Overall volume of less than 7 in^3 (155 cm^3).

* Overall response time of less than 3 ms.

Since exotic propellants or materials are not needed to reduce the projectile mass to make it consistent with that desired for adequate kinetic energy to produce a kill low cost options are available. Low cost would enable adequate proliferation for high coverage.

By being able to control a completely non-electronic "smart rock", the option may be opened to alternative launch mechanisms, particularly that by electro-magnetic rail gun. A projectile that has a mass just equal to that required for kill would not have additional mass and hence would not require the additional

power that has up until now restricted the consideration of EM railguns. The ability of the fluidics to withstand the extremely high magnetic fluxes and enormously high acceleration forces with impunity also contribute to the viability of an EM railgun.

The feasibility of the two systems has other implications. Conventional electromagnetic valves can be replaced by the lighter fluidic systems. Additional guidance can be provided to reduce the burden and expense of precision gimbals or high resolution homing systems. Since the fluidic detection system operates with an electro-optical input (laser energy) electronic inputs can be readily interfaced in by an optically encoded signal transmitted through an optical fiber.

In conclusion, therefore, a feasible technological option for a low cost, light weight, responsive control of KEW projectiles has been presented and should be demonstrated in a full-up test program which is being proposed in the following sections.

7. RECOMMENDATIONS FOR PHASE II EFFORTS

Defense Research Technologies, Inc. recommends that in order to demonstrate the weight, cost and reliability attributes of fluidic technology in the guidance of KEW projectiles in a full-up test program that certain technical challenges identified in the Phase I efforts be addressed.

The main technical objective of the Phase II efforts of this program should, therefore, be to demonstrate the performance of the fluidic guidance components designed and examined in the Phase I of this program, using realistic warm gas propellants.

In addition, the two sub-systems, the laser detection/control system and the diverter/thruster, should be evaluated separately from each other so as to determine the benefits of each alone.

One of the principal conclusions from the Phase I work was that one of the most important parameters affecting the operation of the fluidic elements was the source of power and that the signal processing circuitry probably needs a cold gas source or at least a cooled target area for good sensitivity. Since weight is a critical issue in any KEW projectile, the use of cooled propellant bleed flow needs to be examined in detail, or possibly direct cooling of the target laminations.

7.1 Development of a Laser Detector Power Supply

The fluidic circuits designed and developed in Phase I have been designed to operate primarily with gaseous media having the properties of cold air. The laser detection process by the photo-acoustic effect is most dependent on low temperature operation for its sensitivity. The significant weight saving advantages that fluidics offers would be achieved if no external gas source were to be required. Therefore, operation with bleed flow off the propulsion/thruster motor is the most logical.

A combined radiative and throttling heat exchanger is a reasonable option to examine. A simple, first order analysis of the radiative heat exchange from a flowing gas in a tube shows the principal design parameters that need to be examined.

Given that the heat lost from a lengthwise differential element of low thermal conductivity gas, with a specific heat capacity of c_p and a mass flow rate of m, in a high thermal conductivity tube can be approximated by the radiation loss to absolute zero from the tube surface at the local temperature T, as shown in figure 44, then the governing differential equation for lengthwise temperature along the length of the tube is given by equation 24.

$$dT/dx = - 2\pi r\sigma\ T^4/[mc_p] \quad \ldots\ldots\ldots\ldots\ldots\ldots\ldots\ (24)$$

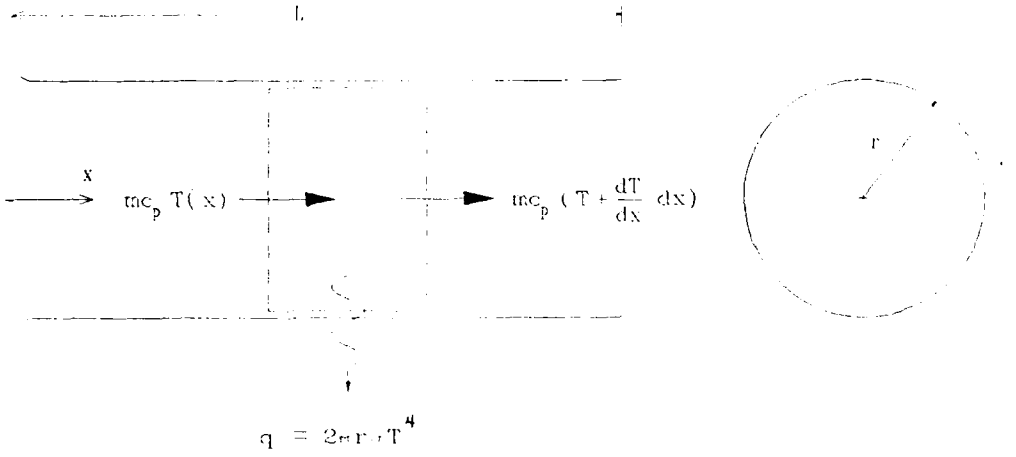

Figure 44. Differential fluid element in heat exchanger tube.

Equation 24 has a closed form solution for the temperature at the end of the tube:

$$T_L = [2\pi r\sigma L/m/c_p + 1/T_o^3]^{-1/3} \quad \ldots\ldots\ldots\ldots\ldots\ldots \quad (25)$$

where:

- r - tube radius
- σ - Stefan-Boltzman constant
- m - mass flow rate
- c_p - gas specific heat capacity at constant pressure
- T_o - temperature at tube inlet.

From this one can see that to minimize T_L the mass flow has to be small, the tube length needs to be long and the tube radius should be large.

There can be cooling due to isentropic throttling which follows the general form of:

$$T_1/T_o = [P_1/P_o]^{(k-1)/k} \quad \ldots\ldots\ldots\ldots\ldots\ldots\ldots\ldots \quad (26)$$

where the subscript "1" denotes the downstream condition and "o" the upstream condition and k is the ratio of specific heats. For $k = 1.2$ the downstream absolute temperature can be as low as 0.44 of the upstream temperature when the gas is expanded from 2000 psia to 15 psia.

A heat exchanger located on the outside of the projectile would appear to be a logical solution.

Filtration of any solid particles from the gas generator will need to be considered.

The heat exchanger will have to be designed of a refractory material that can withstand the erosion and high temperature of the warm gasses. Since high thermal conductivity is of significant concern a tube construction of metal, for strength, coated internally with a thin layer of either MgO or BeO will be considered.

7.2 Development of Lightweight, Space-Worthy Hardware

The fluidic circuitry required to provide the laser detection function, signal processing and logic has already been built and demonstrated on cold gas. The standard Government C/2-format has shown itself to be versatile and adequate for the job. Some slight level of optimization is recommended, however, to reduce the number of laminations required thereby further reducing the weight of system. Recommended stacking improvements include the design and fabrication of precision resistor elements which would eliminate the need for multiple parallel stacks that are currently needed to develop a given desired resistance value from standard resistor elements. In addition, customized manifolding laminations, which connect the desired holes, should be designed to eliminate the need for multiple laminations per interconnection. The principal effort, however, should be to manufacture all the C/2-format laminations in lightweight graphite or carbon-carbon composite. As mentioned before graphite LPA elements have been successfully fabricated in the past. Both fine-blanking (an ultra-high precision punch and die process developed in Switzerland) and laser machining have been used however, for the scope of a Phase II program fine-blanking would be far too expensive to consider for any laminates other than the LPAs themselves, because of the large number of different topologies required. Defense Research Technologies, Inc. has had sample graphite elements cut by using EDM (electro-discharge machining) and this would be the recommended approach.

It is further recommended that the performance parameters be established when hot or warm gasses are used as the working medium.

7.3 Development/Fabrication of Diverter Valve Hardware

The two-axis, four-way valve, as well as a two-way, single axis valve should be built to the specifications identified in the design procedure developed in Phase I. The valve, shown in the engineering drawing of figure 43, should be fabricated in two materials, low temperature and high temperature. The first material should be a conventional low temperature metal, e.g. aluminum, for use with cold gas testing.

Supersonic diverter parameters that will have to be measured and optimized should be -

* Position and angle of oblique shock
* Position of normal shock
* Recovery pressures and flows
* Supply nozzle pressure/flow characteristic
* Switching pressure and flow
* Vortex valve turndown ratio
* Vortex valve supply characteristics
* Bleed channel resistance
* Thrust level
* Response time

All tests need to be performed using actual size hardware because it is well known that complex turbulent, supersonic flows cannot be scaled. The positions and angles of the shocks should be measured using internal flow visualization such as surface oil streaking. The position of the shock appears as a heavy streak of oil on the surface. DC pressure and flow measurements can be made using conventional pressure transducers (flow will be measured as a pressure drop across a resistive element). Response time can be measured using dynamic piezo-electric pressure transducers that trigger a digital oscilloscope. Rise times, delay times can be read directly from the digitized trace.

Once a valve design has been optimized and demonstrated functional on cold gas, the minor design changes required to accommodate hot gas operation ought to be implemented. The major part of the actual efforts will be the development and fabrication of a valve in a material that will withstand warm gas operation for up to 100 seconds and the testing of the valves on warm gasses from a gas generator.

It is anticipated that the valve geometry would be well in hand and that the use of the refractory materials previously identified will be mainly a fabricability problem. At this point in time it is anticipated that the valve body would be metal, probably molybdenum. Hot isostatic processing (HIP) of the powdered metal would appear to be the way to go in production, however, DRT anticipates that the same conventional methods used to fabricate the cold gas models will suffice. The axi-symmetric design of the interaction (switching) region readily lends itself to being turned on a lathe, as do the axi-symmetric components of the vortex valves. All other parts can also be conventionally milled or machined.

A parameter that would have to watched would be the structural integrity of the valve. Erosion, wear and thermal damage to sections would need to be analyzed and alternative materials and geometric configurations examined that could minimize the effects, particularly if they are found to be excessive. The flow visualization experiments from the cold gas testing will also be a good guide as to the location of separation, stagnation and swirling zones where wear and erosion may become a problem. The hot gas

tests will verify if there is a problem. The likely candidate material for the internal coating of the valve is silicon carbide. It is easy to work with, is relatively inexpensive and can readily withstand temperatures up to the rated 3000°F with good oxidation resistance and has extremely good erosion characteristics. In addition, it is readily coated onto graphite and carbon-carbon composites by the high temperature reaction of silicon powder packed against the carbon material.

7.4 Alternative Switching Mechanisms

One of the attractive features of this program is that actually two separable elements are being developed ... the laser guidance package and the diverter valves. In order to make the diverter valves stand alone, actuation means other than fluidic gas injection need to be established and demonstrated. These alternative means have been identified as tab insertion, spark, and secondary fluid injection. It is recommended that valves be designed to accommodate these actuation mechanisms.

Tab insertion can be accomplished by a solenoid activated mechanism into the flow stream. Parameters that will need to be measured are the length of tab required for positive switching, electrical power required, and response time.

Spark initiation can be performed by including two electrodes on the wall. A conventional spark plug design may be a likely candidate. Parameters that will need to be measured are electrode voltage and power required for switching as well as response time.

Secondary fluid injection could be performed by a solenoid activated mechanical valve. It is recommended that only high pressure gas be injected. Parameters that will need to be measured are the pressure and flow required to switch and electrical power requirements. These tests could be performed on the cold gas valves and the most promising chosen for demonstration in one of the hot gas firings.

7.5 Integration of a Complete KEW Guidance System

The laser guidance and the diverters, should integrated together. Figure 45 is a conceptual drawing of both the integrated package and a typical engagement scenario that it would be important to demonstrate.

Performance parameters that will need to be monitored are:

* Response time
* Power consumption
* Thrust level
* Overall mass (weight)
* Size (volume)

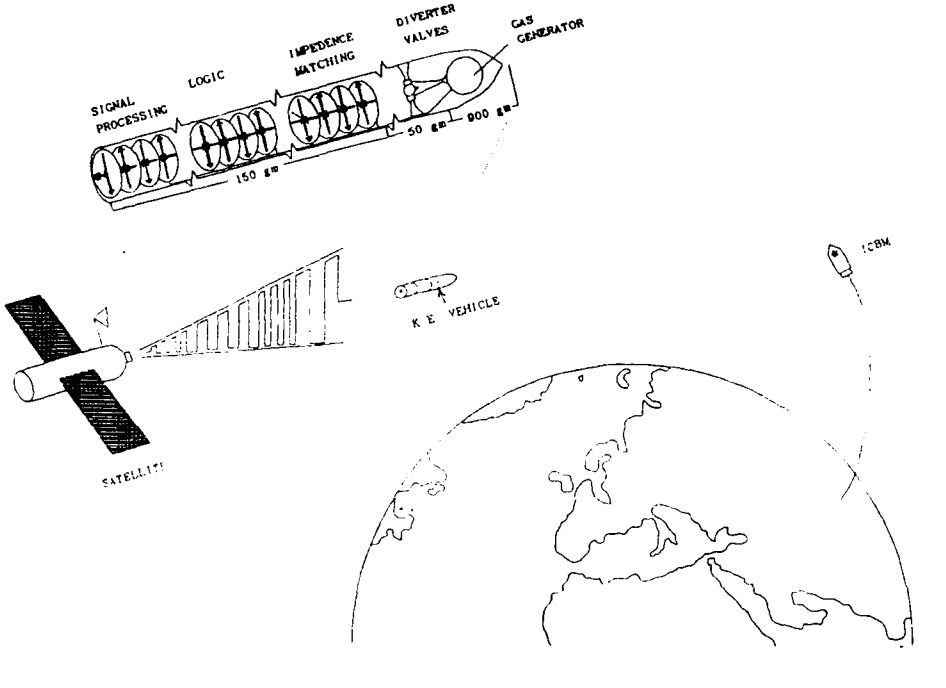

Figure 45. Conceptual integrated KEW projectile.

Performance is not the only parameter that is of interest to the SDI for a KEW projectile. Cost is a big issue. Sufficient information on the fabrication, repeatability, reliability, materials, etc. should be gathered so that a reasonable flyaway cost estimate for an all-fluidic projectile, and individual elements, could be made.

7.6 Potential Commercial Spinoffs

A significant spin-off capability exists in the commercial arena, but has yet to be fully addressed or tapped. The successful demonstration of the sophisticated capabilities of fluidics in a Phase II program would go a long way to reducing risk and opening the door to the commercial market which is in general quite conservative, being driven by quick return and the profit motive. For example, the remote control via laser beam or by optical fiber transmission of mechanical control devices, robotic

elements, and fluid valves in hostile environments is of considerable interest.

Control of nuclear waste valves and radioactive matter flow diverters in nuclear or fusion reactors could be made possible without having to physically penetrate containment vessels or to maintain them by human intervention. Accidents such as Three Mile Island and Chernobyl may in the future be averted because of an increase in system reliability and the ability to provide an increased level of sophistication in the control (e.g. adaptive controllers that need to use computers but normally would have lacked the reliable control links).

Control of the manufacture of explosives and other hazardous or toxic materiel such as munitions, propellants, petro-chemicals, and chemical agents could be performed reliably and remotely. Other applications would become apparent as the technology is exploited.

APPENDIX - Computer Program For Valve Design

```
100 'Program SDIDIVER.BAS
110 'Fluidic Diverter Valve Design
120 'E. Packard
130 'Defense Research Technologies, Inc.
140 'December, 1988
150 '
160 'This program determines the operating characteristics and critical
170 'dimensions for a supersonic fluidic diverter with vortex valves.
180 'Input requirements include supply gas properties, maximum thrust,
190 'diverter deflection angle, vortex valve turn down ratio and ambient
200 'pressure.  Output includes gas properties at several locations in
210 'or around the diverter assembly and the dimensions which correspond
220 'to these properties.
230 '
240 KEY OFF:COLOR 7,1,1:CLS
250 OPEN "LPT1:" FOR OUTPUT AS #1
260 LOCATE 5,1
270 PRINT "
280 PRINT "
290 PRINT "
300 PRINT "
310 PRINT "
320 PRINT "
330 PRINT "
340 PRINT "
390 PRINT "
400 PRINT:PRINT
410 '-------------------------------------------------------------------------
420 'Initial Conditions
430 '
440 PI = 3.141593
450 K = 1.2                          'specific heat ratio (dimensionless)
460 RENG = 53.34                     'gas constant (ft·lbf/lbm·°R)
470   R = RENG * 5.3803              'gas constant (J/kg·K)
480 M0 = 0                           'Mach # of supply
490 P0PSI = 2000                     'supply pressure (psi)
500   P0 = P0PSI * 6895              'supply pressure (N/m²)
510 T0F = 3000                       'supply temperature (°F)
520   T0 = (5/9)*(T0F+459.67)        'supply temperature (°K)
530 TAU1LBF = 10                     'thrust (lbf)
540   TAU1 = TAU1LBF * 4.448         'thrust (N)
550 THETADEG = 12.5                  'deflection angle (degrees)
560   THETA = THETADEG * PI/180      'deflection angle (radians)
570 PAPSI = 0                        'atmospheric pressure (psia)
580   PA = PAPSI * 6895              'atmospheric pressure (N/m²)
590 TR = 10                          'turndown ratio
600 '-------------------------------------------------------------------------
```

SDI DIVERTER VALVE DESIGN

by:

Defense Research Technologies, Inc.

```
610 'Mach Number Iteration
620 'The Mach number at the supply nozzle exit plane is varied incrementally
630 'and all other parameters (dependent on M1) are calculated accordingly.
640 '
650 FOR M1 = 1 TO 5 STEP .1
660   PRINT "Evaluating M1 =";M1
670   '-------------------------------------------------------------------
680   'Oblique Shock Angle Calculations
690   'Given THETA, M1 and K, the oblique shock angle BETA is calculated
700   'by the trial and error method.
710   '
720   FOR BETA = THETA TO 90*PI/180 STEP .005
730     TANTHETA = (2/TAN(BETA))*((M1^2*(SIN(BETA))^2-1) /
                  (M1^2*(K+(COS(BETA))^2)+2))
                                        'Schaum eq. 8.10
740     IF TANTHETA >= TAN(THETA) THEN 760
750   NEXT BETA
760   BETADEG = BETA*180/PI
770   '-------------------------------------------------------------------
780   'Mach Number Calculations
790   '
800   M2 = SQR(((2+(K-1)*M1^2) / (2*K*M1^2*(SIN(BETA))^2-(K-1))) +
           ((2*M1^2*(COS(BETA))^2) / (2+(K-1)*M1^2*(SIN(BETA))^2)))
                                        'Mach # downstream of oblique shock,
810                                     'Fix eq. 6
820   M3 = SQR(((K-1)*M2^2+2)/(2*K*M2^2-(K-1)))
                                        'Mach # in diffuser, Rob. & Crowe eq 12-57
830   '-------------------------------------------------------------------
840   'Area, Mass Flow Rate, and Diameter Calculations
850   '
860   A1ASTAR = 1/M1 * (((1+((K-1)/2)*M1^2)/((K+1)/2))^((K+1)/(2*(K-1))))
                                        'area ratio A1/A* (dimensionless),
                                         Roberson & Crowe eq. 12-56
870   ASTAR = TAU1 / (P0*K*SQR((2/(K-1))*(2/(K+1))^((K+1)/(K-1))) *
              SQR(1-(PA/P0)^((K-1)/K)))
                                        'throat area (m²), Shapiro eq. 4.33
880   ASTARSQIN = ASTAR / 6.4516E-04    'throat area (in²)
890   DSTAR = SQR(4*ASTARSQIN/PI)       'throat diameter (in)
900   MDOT = (P0*ASTAR/SQR(R*T0)) * SQR(K) * (2/(K+1))^((K+1)/(2*(K-1)))
                                        'mass flow rate (kg/s),
                                         Roberson & Crowe eq. 12-58
910   W = MDOT / .45359                 'mass flow rate (lbm/s)
920   A1 = A1ASTAR * ASTAR              'supply nozzle exit area (m²)
930   A1SQIN = A1/6.4516E-04            'supply nozzle exit area (in²)
940   D1 = SQR(4*A1SQIN/PI)             'supply nozzle exit diameter (in)
950   '-------------------------------------------------------------------
960   'Pressure Calculations
970   '
980   P1P0 = ((1+((K-1)/2)*M0^2)/(1+((K-1)/2)*M1^2)) ^ (K/(K-1))
                                        'pressure ratio P1/P0  (dimensionless),
                                         Roberson & Crowe eq. 12-26
990   P1 = P1P0 * P0                    'supply nozzle exit pressure (Pa)
```

```
1000   'Separation pressure ratio P6/P1 is calculated by the trial and error
1010   'method in the following loop.
1020   FOR P6P1 = 1.1 TO 10 STEP .05
1030     EQUALS1 = ((1+((.225*K*M1^2)/(1+((K-1)/2)*M1^2))) *
                   (1+(.18*K*SQR(M1^2-1))/((1+.28*(K-1)*M1^2)*1.2*
                   (P6P1-1))))/P6P1  'Morgan eq. 2.1
1040     IF EQUALS1 <= 1 THEN 1060
1050   NEXT P6P1
1060   P6 = P6P1 * P1                  'separation pressure (Pa)
1070   P2P1 = (2*K)/(K+1) * (M1^2*(SIN(BETA))^2) - (K-1)/(K+1)
                                       'pressure ratio across oblique shock (dim)
                                        Fix eq. 7 and Hallum eq. 1
1080   P2 = P2P1 * P1                  'pressure downstream of oblique shock (Pa)
1090   P3P2 = (1+K*M2^2)/(1+K*M3^2)    'pressrue ratio across normal shock (dim
                                        Roberson & Crowe eq. 12-38
1100   P3 = P3P2 * P2                  'pressure downstream of normal shock (Pa)
1110   PT3 = P3 * (1+((K-1)/2)*M3^2)^(K/(K-1))
                                       'total pressure downstream of normal shock
                                        (Pa), Rob. & Crowe eq. 12-27
1120   P4 = P2                         'off-side pressure equal to on-side static
                                        pressure after oblique shock (Pa)
1130   PT3P4 = PT3/P4                  'on-leg to off-leg pressure ratio (dim)
1140   P0PSI = P0/6895                 'convert from Pa to psi
1150   P1PSI = P1/6895                 'convert from Pa to psi
1160   P2PSI = P2/6895                 'convert from Pa to psi
1170   P3PSI = P3/6895                 'convert from Pa to psi
1180   PT3PSI = PT3/6895               'convert from Pa to psi
1190   P4PSI = P4/6895                 'convert from Pa to psi
1200   P6PSI = P6/6895                 'convert from Pa to psi
1210   '-------------------------------------------------------------------
1220   'Temperature Calculations
1230   '
1240   T1T0 = P1P0^((K-1)/K)           'Roberson & Crowe eq. 12-24
1250   T1 = T1T0 * T0                  'supply nozzle exit gas temperature (°K)
1260   T2T1 = 1 + ((2*(K-1)*M1^2*(SIN(BETA))^2-1)/((K+1)^2*M1^2*(SIN(BETA))^2
              * (K*M1^2*(SIN(BETA))^2+1)
                                       'Schaum eq. 8.7
1270   T2 = T2T1 * T1                  'Temperature after oblique shock (°K)
1280   T3T2 = (1+((K-1)/2)*M2^2) / (1+((K-1)/2)*M3^2)
                                       'Roberson & Crowe eq. 12-39
1290   T3 = T3T2 * T2                  'diffuser gas temperature (°K)
1300   TT3 = T3 * (1+((K-1)/2)*M3^2)   'total temperature of diffuser gas (°K)
1310   T4 = T2                         'off-side gas temperture (°K)
1320   '-------------------------------------------------------------------
1330   'Vortex Valve Data Initialization
1340   '
1350   RHO3 = (PT3/(R*TT3))*.028317/.45359
                                       'on-leg gas density (lbm/ft^3)
1360   RHO4 = (P4/(R*T4))*.028317/.45359
                                       'off-leg gas density (lbm/ft^3)
```

```
1370   WM = W                              'maximum mass flow rate (lbm/s)
1380   ASR = 3                             'supply area ratio As/Ae
1390   HR = 2                              'height ratio h/re
1400   RR = .3                             'radius ratio re/ro
1410   PS = P4PSI-PAPSI                    'supply pressure (psi)
1420   PCC = PT3PSI-PAPSI                  'cutoff control pressure (psi)
1430   PR = PCC/PS                         'pressure ratio
1440   '-------------------------------------------------------------------
1450   'Vortex Valve Calculations
1460   '
1470   AE = (WM*12)/(.75*SQR(2*RHO3*PT3PSI/32.2)*32.2)
                                           'exit port area (in²)
1480   RE = SQR(AE/3.14159)                'exit radius (in)
1490   DE = 2 * RE                         'exit diameter (in)
1500   WMOFF = (AE*.75*SQR(2*RHO4*P4PSI/32.2)*32.2)/12
                                           'mass flow rate of off-leg with vortex
                                            valve open (lbm/s)
1510   WCC = WMOFF / TR                    'min weight flow rate (lbm/sec)
1520   WR = WCC / WM                       'weight flow ratio
1530   QCC = (1728*WCC) / RHO3             'minimum volumetric flow rate (in^3/sec
1540   A5AE = 50                           'thrust nozzle exit area to throat area
                                            ratio A5/AE (dimensionless)
1550   A5 = A5AE * AE                      'thrust nozzle exit area (in²)
1560   D5 = SQR(4*A5/PI)                   'thrust nozzle exit diameter (in)
1570   AS = AE * ASR                       'supply area to vortex valve (in²)
1580   H = HR * RE                         'height of vortex valve chamber (in)
1590   AC = (WCC*12)/(.75*SQR((2*RHO3*PCC)/32.2)*32.2)
                                           'control area (in²)
1600   DC = SQR(4*AC/PI)                   'control diameter (in)
1610   ACR = AC / AE                       'control area ratio Ac/Ae
1620   RO = RE / RR                        'outer radius of vortex valve chamber (in)
1630   DO = 2 * RO                         'outer dia. of vortex valve chamber (in)
1640   AO = (PI*DO^2)/4                    'area of vortex vave chamber (in²)
1650   ACB = AO - AS                       'area of center body (in²)
1660   DCB = SQR(4*ACB/PI)                 'diameter of center body (in)
1670   EFF = (WM-2*WCC)/WM                 'efficiency of single axis diverter
1680   EFF22 = (WM-(2*WCC+.5*WM))/WM       'efficiency of two single axis diverter
1690   EFF4 = (WM-4*WCC)/WM                'efficiency of one dual axis diverter
1700   '-------------------------------------------------------------------
1710   'Output
1720   '
1730   PRINT#1, "INPUT:"
1740   PRINT#1,
1750   PRINT#1, "  k  =";K
1760   PRINT#1, "  R  =";RENG;"ft·lbf/lbm·°R"
1770   PRINT#1, "  P0 =";P0PSI;"psi"
1780   PRINT#1, "  T0 =";T0F;"°F"
1790   PRINT#1, "  M0 =";M0
1800   PRINT#1, "  T  =";TAU1LBF;"lbf"
1810   PRINT#1, "  Θ  =";THETADEG;"°"
1820   PRINT#1, "  TR =";TR
1830   PRINT#1, "  M1 =";M1
1840   PRINT#1,
```

```
1850    PRINT#1, "OUTPUT:"
1860    PRINT#1,
1870    PRINT#1, "  M2 =";M2
1880    PRINT#1, "  M3 =";M3
1890    PRINT#1, "  W  =";W;"lbm/sec"
1900    PRINT#1, "  β  =";BETADEG;"°"
1910    PRINT#1, "  η  =";EFF
1920    PRINT#1,
1930    PRINT#1, "Pressures:"
1940    PRINT#1, "  P1  =";P1PSI;"psi"
1950    PRINT#1, "  P2  =";P2PSI;"psi"
1960    PRINT#1, "  P3  =";P3PSI;"psi"
1970    PRINT#1, "  Pt3 =";PT3PSI;"psi"
1980    PRINT#1, "  P4  =";P4PSI;"psi"
1990    PRINT#1, "  Pt3/P4 =";PT3P4
2000    PRINT#1, "  P5  =";P5PSI;"psi"
2010    PRINT#1, "  P6  =";P6PSI;"psi"
2020    PRINT#1, "  P6/P1 =";P6P1
2030    PRINT#1,
2040    PRINT#1, "Vortex Valve:"
2050    PRINT#1, "  Ps  =";PS;"psi
2060    PRINT#1, "  Pcc =";PCC;"psi
2070    PRINT#1, "  PR  = Pcc/Ps =";PR
2080    PRINT#1, "  Wm  =";WM;"lbm/sec"
2090    PRINT#1, "  Wcc =";WCC;"lbm/sec"
2100    PRINT#1, "  re/ro =";RR
2110    PRINT#1, "  Ac/Ae =";ACR
2120    PRINT#1, "  As/Ae =";ASR
2130    PRINT#1, "  h/re  =";HR
2140    PRINT#1,
2150    PRINT#1, "Dimensions:"
2160    PRINT#1, "  A*  =";ASTARSQIN;"in²"
2170    PRINT#1, "  A1  =";A1SQIN;"in²"
2180    PRINT#1, "  A1/A* =";A1ASTAR
2190    PRINT#1, "  As  =";AS;"in²"
2200    PRINT#1, "  Ac  =";AC;"in²"
2210    PRINT#1, "  Ae  =";AE;"in²"
2220    PRINT#1, "  A5  =";A5;"in²"
2230    PRINT#1, "  A5/Ae =";A5AE
2240    PRINT#1, "  H   =";H;"in"
2250    PRINT#1, "  D*  =";DSTAR;"in"
2260    PRINT#1, "  D1  =";D1;"in"
2270    PRINT#1, "  Do  =";DO;"in"
2280    PRINT#1, "  Dcb =";DCB;"in"
2290    PRINT#1, "  Dc  =";DC;"in"
2300    PRINT#1, "  De  =";DE;"in"
2310    PRINT#1, "  D5  =";D5;"in"
2320    PRINT#1,CHR$(12)                    'form feed
2330 NEXT M1                                'end loop
2340 BEEP
```